Experimental and Theoretical Study of the Ag-Sn-Te Phase Diagram

Sinn-wen Chen[1,2] · Aleš Kroupa[3] · Jia-yu Du[1] · Adéla Zemanová[3] ·
Yohanes Hutabalian[1] · Jan Vřešťál[3] · Kuo-chun Chiu[1]

Abstract Experimental and theoretical study of the Ag- Sn-Te system was carried out in the scope of the study. The isothermal sections at 350 and 500 °C were studied experimentally. The results were used together with other experimental data from the literature for the theoretical assessment of the system by the *CALPHAD* method. Generally, a very good agreement was obtained both for the phase diagram and for the enthalpies of mixing in the liquid phase. The existence of the ternary phase ($Ag_xSn_{2-x}Te_2$) was confirmed, and a slightly different composition ($x = 0.8$) was evaluated in the experimental part of the study.

Keywords Ag-Sn-Te system · Experimental phase equilibria · CALPHAD method · SEM · Theoretical assessment · XRD

1 Introduction

Thermoelectric materials and devices have attracted tremendous research efforts due to their very promising potentials in energy-related applications.[1–3] Various

✉ Aleš Kroupa
kroupa@ipm.cz

Sinn-wen Chen
swchen@mx.nthu.edu.tw

1   Department of Chemical Engineering, National Tsing Hua University, Hsinchu 300, Taiwan

2   High Entropy Materials Center, National Tsing Hua University, Hsinchu 300, Taiwan

3   Institute of Physics of Materials, Czech Academy of Sciences, Zizkova 22, 61662 Brno, Czech Republic

thermoelectric materials have been investigated. Ag_2Te, SnTe and PbTe compounds are among those mostly studied.[4–12] The studies of the influence of doping and microstructural engineering on the thermoelectric properties of these three compounds are also very frequent as part of the development effort. The material systems involved in such studies include Ag-Sn-Te,[7,8] Ag-Sb-Sn-Te,[9,10] Ag-Pb-Sn-Te[11] Ag-Pb-Sb-Sn-Te,[12] etc. Ag-Sn-Te is the sub-system for most of these multicomponent systems.[4–12] Therefore, it is very important to know the behavior and properties of this system for the development of thermoelectric applications.

Phase diagrams represent an effective way for phase equilibria description, which are fundamentally important for understanding the properties of complex multicomponent materials.[13-15] Vertical sections of Ag-Sn-Te system were determined by Blachnik et al.[16] and Blachnik and Gather.[17] Ag-Sn-Te liquidus projection were determined by Chang et al.[18] and Blachnik et al.[16] The existence of the ternary compound $AgSnTe_2$ has been confirmed.[16,19] The thermodynamic properties, specifically the enthalpies of mixing of liquid were measured in.[20,21] Although these experimental results are available,[16–21] the Ag-Sn-Te phase diagram for the range of compositions and temperatures of interest for thermoelectric applications is missing.

Phase diagrams can be determined by experimental measurements and theoretical modelling (e.g., *CALPHAD*-type calculations).[13–15] In this study, equilibrium Ag-Sn-Te ternary alloys were prepared and isothermal sections of the Ag-Sn-Te phase diagram at 350 and 500 °C were determined experimentally. Subsequently, the modeling of the ternary Ag-Sn-Te system using the CALPHAD method was performed based on own experimental results, phase data evaluated from the literature,[16–19] thermodynamic

140

J. Phase Equilib. Diffus. (2022) 43:139–163

data for the system Ag-Sn-Te[20,21] and thermodynamic evaluations of relevant binary systems.[22–24]

2 Experimental Procedures

The Ag-Sn-Te ternary alloys were prepared from pure elements, Ag shots (99.9 wt.%, Alfa Aesar, USA), Sn shots (99.95 wt.%, Showa, Japan) and Te shots (99.99 wt.%, Gredmann, Taiwan). The correct amounts of pure components with a total amount of one gram were prepared and sealed in a quartz tube under a reduced pressure of 3×10^{-2} mbar. The samples were heated up to 1000 °C at a 10 °C/min heating rate, homogenized for 3 hours and then quenched in water. The alloys were then equilibrated at 350 and 500 °C for 180 days.

The equilibrated samples were removed from quartz tubes after annealing and cut in half. One half of the sample was mounted, polished and metallographically analyzed. The microstructures and compositions of the phases were determined by using Scanning Electron Microscopy (SEM, Hitachi S-2500, Japan) and Electron Probe Microanalysis (EPMA, Joel JAX-8600SX, Japan). Second half of the sample was prepared for powder x-ray Diffraction Analysis (XRD, Scintac, XDS-2000V/H, USA), and the phases were identified based on JCPDS (Joint Committee of Powder Diffraction standard).

3 Experimental Results

3.1 Ag-Sn-Te Isothermal Section at 350 °C

As shown in Table 1 and Fig. 1, 38 Ag-Sn-Te alloys were prepared. In the Ag-Sn binary system, there are two stable binary compounds at 350 °C, ζ-Ag$_4$Sn and ε-Ag$_3$Sn[18]. There are also binary compounds in the Ag-Te binary system[24], namely Ag$_2$Te, Ag$_{1.9}$Te and Ag$_5$Te$_3$, each with several temperature modifications. There is one stable compound, SnTe, in the binary Sn-Te system[17]. All samples were equilibrated for 180 days at this temperature.

3.1.1 (Ag)+β-Ag$_2$Te

The structure of alloy #1 (Ag-5.0 at.% Sn-5.0 at.% Te) using backscattered electrons image (BEI) is shown in Fig. 2(a). Two phases were observed. The composition of the light phase is Ag-32.8 at.% Te with a negligible amount of Sn and it is likely the β-Ag$_2$Te phase. The composition of the dark matrix phase is Ag-5.9 at.% Sn-0.5 at.% Te and corresponds to the (Ag) solid solution. The relevant x-ray pattern is shown in Fig. 2(b), and the diffraction peaks corresponding to the β-Ag$_2$Te and Ag

phases were identified. The results of microstructural analysis, compositional measurements and x-ray diffraction are consistent and the microstructure of alloy #1 consists of the (Ag)+β-Ag$_2$Te two-phase region. Similar results are observed for alloy #27 (Ag-5.0 at.% Sn-10.0 at.% Te).

3.1.2 ζ-Ag$_4$Sn+ β-AgTe

The BEI micrograph of the equilibrated microstructure of alloy #30 (Ag-15.0 at.% Sn-5.0 at.% Te) is shown in Fig. 3(a). Two phases are observed. The composition of the bright phase is Ag-34.7 at.% Te without noticeable amount of Sn, and it is likely to be the β-Ag$_2$Te phase. The composition of the dark matrix phase is Ag-16.3 at.% Sn-0.3 at.% Te. It corresponds to the ζ-Ag$_4$Sn phase with 0.3 at.% Te solubility. The x-ray diffractogram is shown in Fig. 3(b). The diffraction peaks of β-Ag$_2$Te and ζ-Ag$_4$Sn phases are identified there. The x-ray results are consistent with the compositional analysis. Alloy #30 lies in the two-phase ζ-Ag$_4$Sn+β-Ag$_2$Te field at 350 °C. Similar results were obtained for alloy #28 (Ag-5.0 at.% Sn-25.0 at.% Te). Alloy #28 is also in the ζ-Ag$_4$Sn+β-Ag$_2$Te two-phase field.

No reliable experimental results were obtained for the three-phase ζ-Ag$_4$Sn+β-Ag$_2$Te+SnTe region.

3.1.3 ζ-Ag$_4$Sn+ SnTe

The BEI micrograph presents the microstructure of alloy #31 (Ag-25.0 at.% Sn-10.0 at.% Te) in Fig. 4(a). Two phases were observed. The composition of the bright phase is Ag-49.1 at.% Sn-50.1 at.% Te. It corresponds to the SnTe phase with 0.8 at.% Ag solubility. The composition of the gray phase is Ag-17.4 at.% Sn-0.4 at.% Te. This is the ζ-Ag$_4$Sn phase with small Te solubility. The x-ray diffractogram is presented in Fig. 4(b). The diffraction peaks of SnTe and ζ-Ag$_4$Sn phases were identified. The results are consistent with the compositional analysis. Alloy #31 lies in the ζ-Ag$_4$Sn+SnTe two-phase field. Similar results were observed for alloy #19 (Ag-45.0 at.% Sn-45.0 at.% Te). The alloy #19 is also in the ζ-Ag$_4$Sn+SnTe two-phase field.

No experimental sample showed the three-phase ζ-Ag$_4$Sn+ε-Ag$_3$Sn+SnTe region.

3.1.4 ε-Ag$_3$Sn+SnTe+Liquid

The BEI micrograph of alloy #7 (Ag-35.0 at.% Sn-15.0 at.% Te) is presented in Fig. 5(a). Three phases are observed. The composition of the bright phase is Sn-50.1 at.% Te with negligible Ag solubility and it corresponds to the SnTe phase. The composition of the dark

Table 1 Nominal composition and equilibrium phases of Ag-Sn-Te alloys equilibrated at 350 °C

Alloy no.	Nominal composition (at.%)			Composition equilibrium (at.%)			
	Ag	Sn	Te	Phase	Ag	Sn	Te
1.	90	5	5	Ag$_2$Te	67.2	…	32.8
				Ag	93.6	5.9	0.5
2.	70	25	5	Ag$_3$Sn	74.5	23.1	2.4
				SnTe	1.2	48.8	50.0
3.	70	15	15	Ag$_4$Sn	82.3	17.3	0.4
				Ag$_2$Te	65.6	…	34.4
				SnTe	1.4	48.5	50.1
4.	60	5	35	Ag$_4$Sn	80.2	19.3	0.5
				Ag$_2$Te	65.6	0.3	34.1
				SnTe	1.3	50.0	48.7
5.	60	35	5	Liquid	1.4	97.1	1.5
				SnTe	0.2	50.2	49.6
				Ag$_3$Sn	74.6	24.7	0.7
6.	50	45	5	Liquid	…	95.3	4.7
				SnTe	0.5	50.3	49.2
				Ag$_3$Sn	74.6	25.4	…
7.	50	35	15	Liquid	2.8	95.5	1.7
				SnTe	…	50.1	49.9
				Ag$_3$Sn	74.6	24.9	0.5
8.	40	15	45	Ag$_5$Te$_3$	63.8	…	36.2
				AgSnTe$_2$	19.2	28.4	52.4
9.	30	55	15	Liquid	0.3	98.4	1.3
				SnTe	0.3	50.4	49.3
				Ag$_3$Sn	73.9	25.7	0.4
10.	30	25	45	Ag$_2$Te	64.4	…	35.6
				SnTe	…	49.8	50.2
				AgSnTe$_2$	15.8	33.6	50.6
11	30	15	55	Ag$_5$Te$_3$	63.2	…	36.8
				Liquid	…	…	…
				AgSnTe$_2$	19.3	30.0	50.7
12	20	65	15	Liquid	1.6	95.2	3.2
				SnTe	0.1	50.5	49.4
				Ag$_3$Sn	74.7	25.3	…
13	20	45	35	Liquid	4.3	94.3	1.4
				SnTe	0.1	48.7	51.2
				Ag$_3$Sn	75.1	24.4	0.5
14	20	35	45	Ag$_2$Te	66.0	…	34.0
				SnTe	1.2	48.5	50.3
				Ag$_4$Sn	81.8	17.6	0.6
15	10	85	5	Liquid	0.4	98.1	1.5
				SnTe	0.1	50.4	49.5
16	10	75	15	Liquid	1.7	96.9	1.4
				SnTe	0.2	50.5	49.3
17	10	65	25	Liquid	1.9	97.2	0.9
				SnTe	…	49.6	50.4
				Ag$_3$Sn	75.6	24.0	0.4
18	10	55	35	Liquid	3.1	96.9	…

Table 1 continued

Alloy no.	Nominal composition (at.%)			Composition equilibrium (at.%)			
	Ag	Sn	Te	Phase	Ag	Sn	Te
				SnTe	0.1	50.9	49.0
				Ag$_3$Sn	74.4	25.6	…
19	10	45	45	SnTe	2.6	48.8	48.6
				Ag$_4$Sn	80.9	18.8	0.3
20	10	25	65	Te	0.2	…	99.8
				AgSnTe$_2$	19.2	28.7	52.1
				SnTe	…	…	…
21	10	15	75	Te	…	…	100.0
				AgSnTe$_2$	19.4	29.8	50.8
22	20	5	75	Te	0.1	…	99.9
				AgSnTe$_2$	20.1	28.7	51.2
				Liquid	…	…	…
23	45	45	10	Liquid	3.8	95.3	0.9
				SnTe	0.2	47.4	52.4
				Ag$_3$Sn	74.3	25.3	0.4
24	35	55	10	Liquid	8.1	91.1	0.8
				SnTe	…	49.2	50.8
				Ag$_3$Sn	75.6	24.0	0.4
25	25	70	5	Liquid	4.3	94.9	0.8
				SnTe	…	49.6	50.4
				Ag$_3$Sn	76.1	23.6	0.3
26	35	30	35	Ag$_4$Sn	82.1	17.3	0.6
				Ag$_2$Te	65.9	…	34.1
				SnTe	1.2	48.7	50.1
27	85	5	10	Ag$_2$Te	66.9	…	33.1
				Ag	90.7	8.8	0.5
28	70	5	25	Ag$_2$Te	65.6	…	34.4
				Ag$_4$Sn	82.7	17.0	0.3
29	65	15	20	Ag$_4$Sn	81.2	16.9	1.9
				Ag$_2$Te	64.9	…	35.1
				SnTe	1.6	47.3	51.1
30	80	15	5	Ag$_2$Te	65.3	…	34.7
				Ag$_4$Sn	83.4	16.3	0.3
31	65	25	10	SnTe	0.8	49.1	50.1
				Ag$_4$Sn	82.2	17.4	0.4
32	50	10	40	Ag$_{1.9}$Te	65.0	…	35.0
				AgSnTe$_2$	17.3	31.4	51.3
				Ag$_5$Te$_3$	62.0	…	38.0
33	55	10	35	Ag$_2$Te	65.2	…	34.8
				Ag$_4$Sn	80.4	17.5	2.1
				SnTe	1.3	50.0	48.7
34	25	35	40	Ag$_2$Te	64.7	…	35.3
				Ag$_4$Sn	82.9	16.7	0.4
				SnTe	1.8	47.4	50.8
35	5	5	90	Liquid	…	…	…
				Te	…	…	100.0
				AgSnTe$_2$	18.2	29.8	52.0

Table 1 continued

Alloy no.	Nominal composition (at.%)			Composition equilibrium (at.%)			
	Ag	Sn	Te	Phase	Ag	Sn	Te
36	35	50	15	Liquid	8.1	91.1	0.8
				SnTe	…	49.5	50.5
				Ag$_3$Sn	75.3	24.3	0.4
37	55	30	15	Ag$_3$Sn	74.7	23.0	2.3
				SnTe	0.4	49.1	50.5
38	20	30	50	AgSnTe$_2$	19.5	29.8	50.7
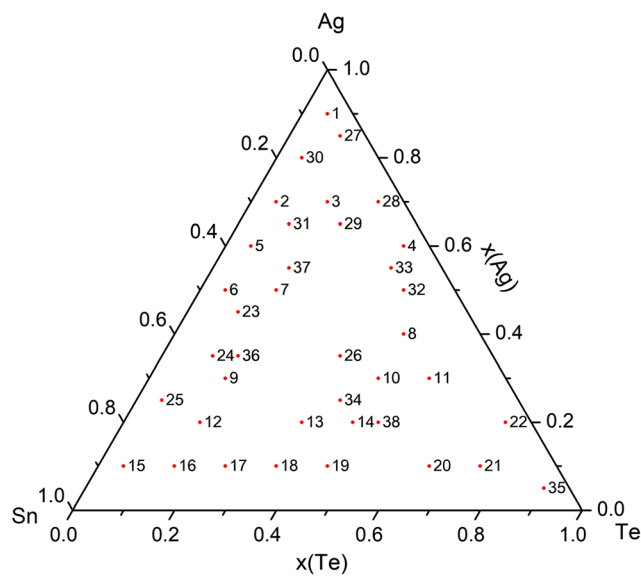
Fig. 1 Prepared and equilibrated alloys of Ag-Sn-Te annealed at 350 °C for 180 days

phase is Ag-24.9 at.% Sn-0.5 at.% Te. It corresponds to the ε-Ag$_3$Sn phase with 0.5 at.% Te solubility. The gray matrix contains a mixture of several phases with very fine morphology. The average composition of this phase is Ag-95.5 at.% Sn-1.7 at.% Te. Based on the results of compositional and microstructural analysis, it is clear that this phase was a liquid phase at 350 °C and solidified into this fine structure when the sample was quenched. The x-ray diffractogram is shown in Fig. 5(b). The diffraction peaks of ε-Ag$_3$Sn, SnTe and Sn phases are identified. The results are consistent with the compositional analysis and alloy #7 lies in the ε-Ag$_3$Sn+SnTe+Liquid three-phase field. Similar results are observed for alloys #5, 6, 9, 12, 13, 17, 18, 23, 24, 25 and 36. The ε-Ag$_3$Sn+SnTe+Liquid three-phase field is very well defined by these samples at this temperature.

3.1.5 SnTe+Liquid

The BEI micrograph of alloy #15 (Ag-85.0 at.% Sn-5.0 at.% Te) is presented in Fig. 6(a). Two phases are observed in the structure. The composition of the bright phase is Ag-50.4 at.% Sn-49.5 at.% Te and defines the SnTe phase with a very small solubility of 0.1 at.% Ag. The darker matrix with fine structure contains several phases and its average composition is Ag-98.1 at.%Sn-1.5 at.%Te. Based on the results of compositional and microstructural analysis, this phase was liquid at 350 °C and decomposed when the sample solidified. The x-ray diffractogram is shown in Fig. 6(b). The diffraction peaks of SnTe and Sn phases are identified. The results are consistent with the compositional analysis. The alloy #15 is in the SnTe+Liquid two-phase field and ε-Ag$_3$Sn and Sn phases were formed during solidification. Similar results are observed for alloy #16.

3.1.6 Ag$_x$Sn$_{2-x}$Te$_2$

The microstructure of alloy #38 (Ag-30.0 at.% Sn-50.0 at.% Te) is presented in Fig. 7(a). Only one phase is observed in the structure. The x-ray diffractogram is presented in Fig. 7(b). The diffraction peaks of the Ag$_x$Sn$_{2-x}$Te$_2$ ternary phase are identified, where x=0.8.

3.1.7 Ag$_x$Sn$_{2-x}$Te$_2$+(Te)+Liquid

The microstructure of alloy #35 (Ag-5.0 at.% Sn-90.0 at.% Te) is presented in Fig. 8(a). Three phases are observed. The composition of the dark phase (Ag-29.8 at.% Sn-52.0 at.% Te) corresponds to the Ag$_x$Sn$_{2-x}$Te$_2$ phase. The composition of the bright phase corresponds to pure Te. The morphology of the gray phase consisting of a fine mixture of phases indicates that it was liquid phase at the annealing temperature. However, no reliable EPMA measurement of this phase is available. Based on the literature,[16,18] the liquid composition should
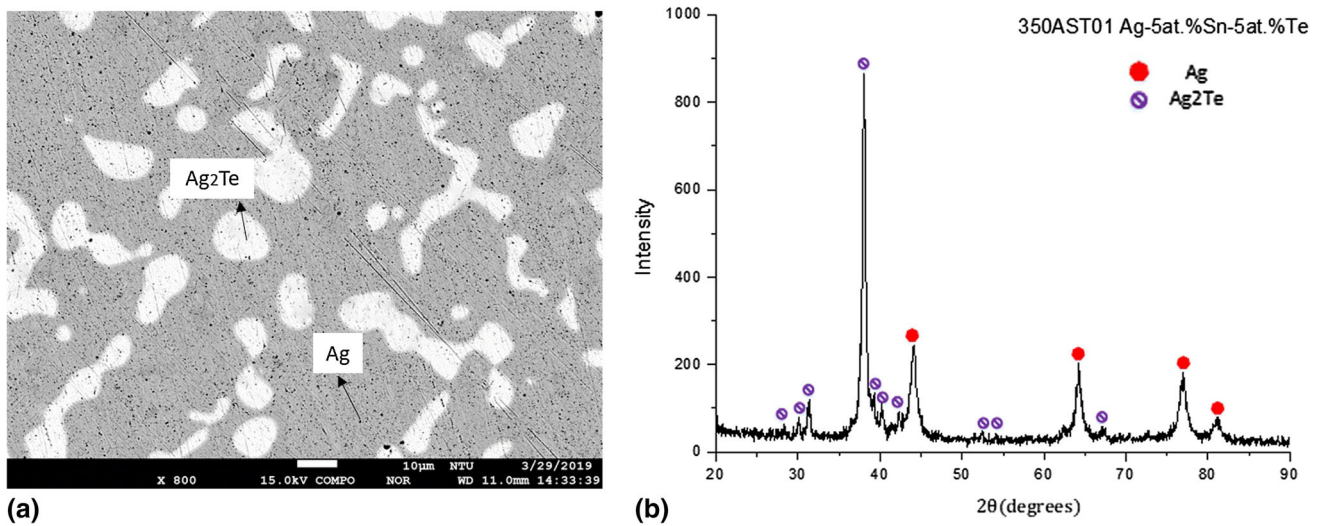
Fig. 2 Alloy #1 (Ag-5.0at.%Sn-5.0at.%Te) equilibrated at 350 °C (a) BEI micrograph (b) x-ray powder diffractogram
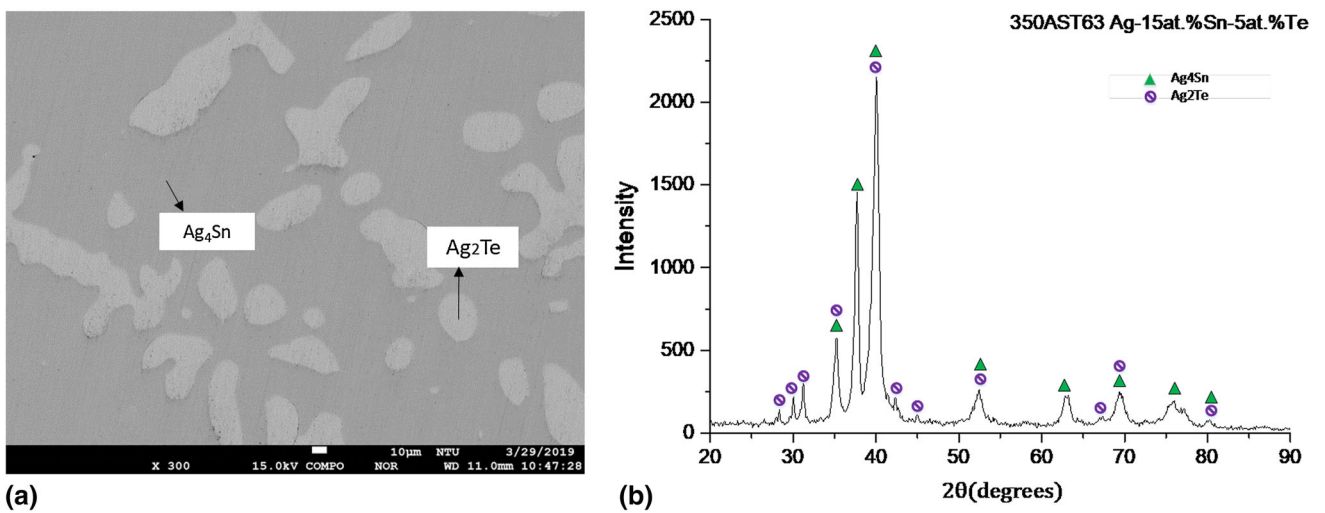

Fig. 3 Alloy #30 (Ag-15.0at.%Sn-5.0at.%Te) equilibrated at 350 °C (a) BEI micrograph (b) x-ray powder diffractogram
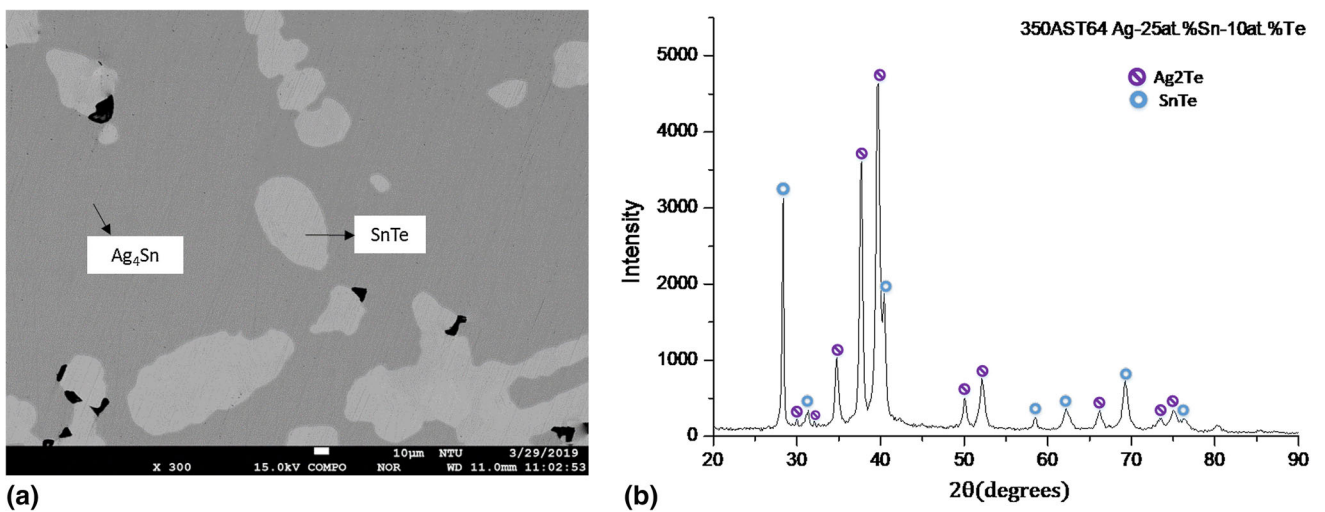

Fig. 4 Alloy #31 (Ag-25.0at.%Sn-10.0at.%Te) equilibrated at 350 °C (a) BEI micrograph (b) x-ray powder diffractogram
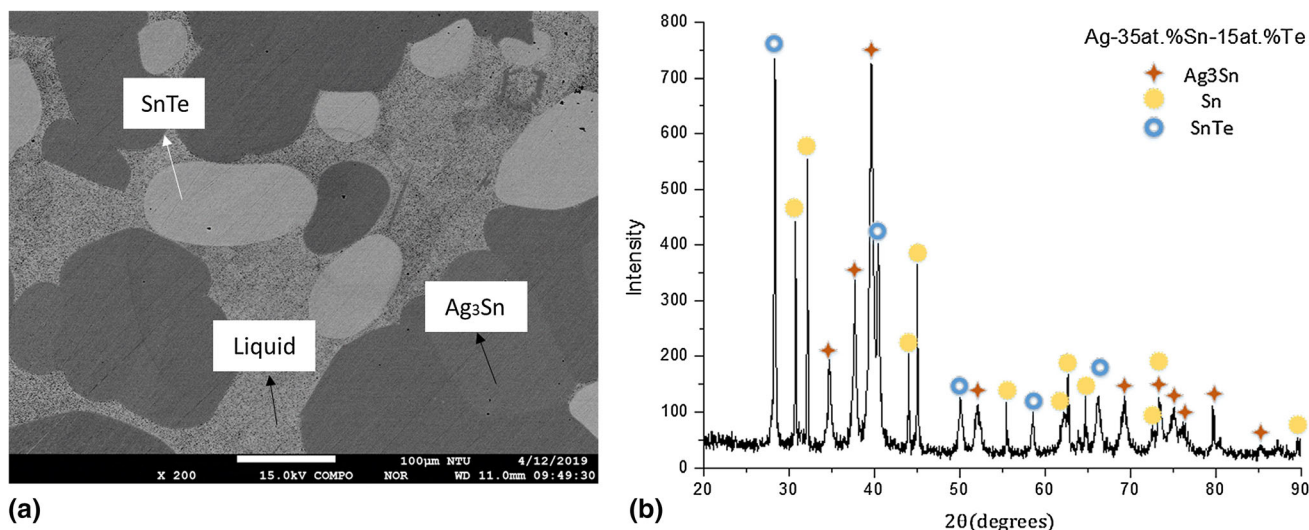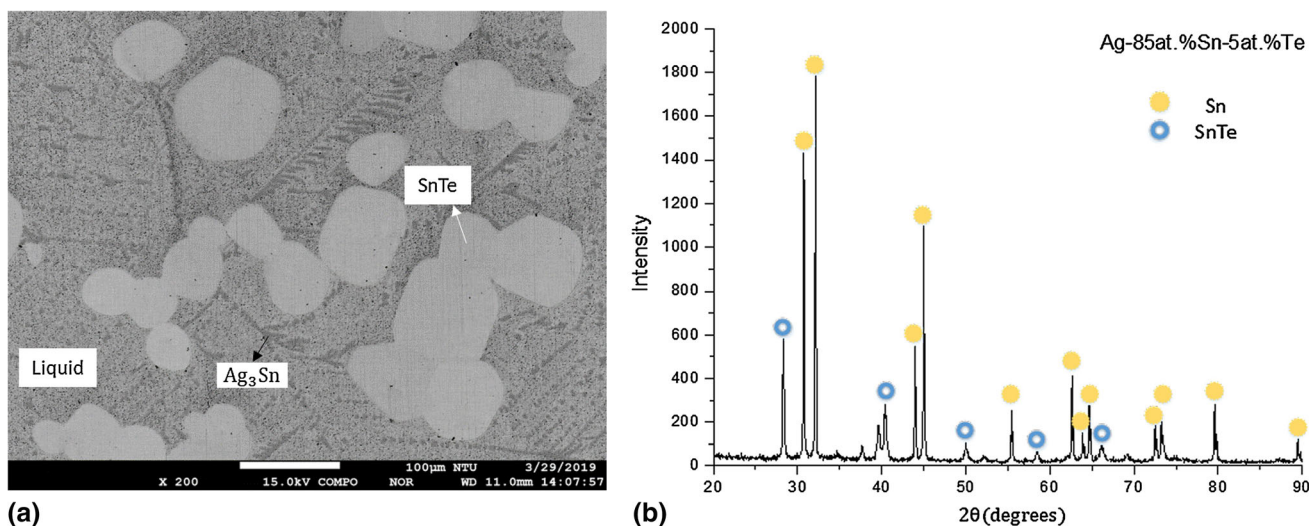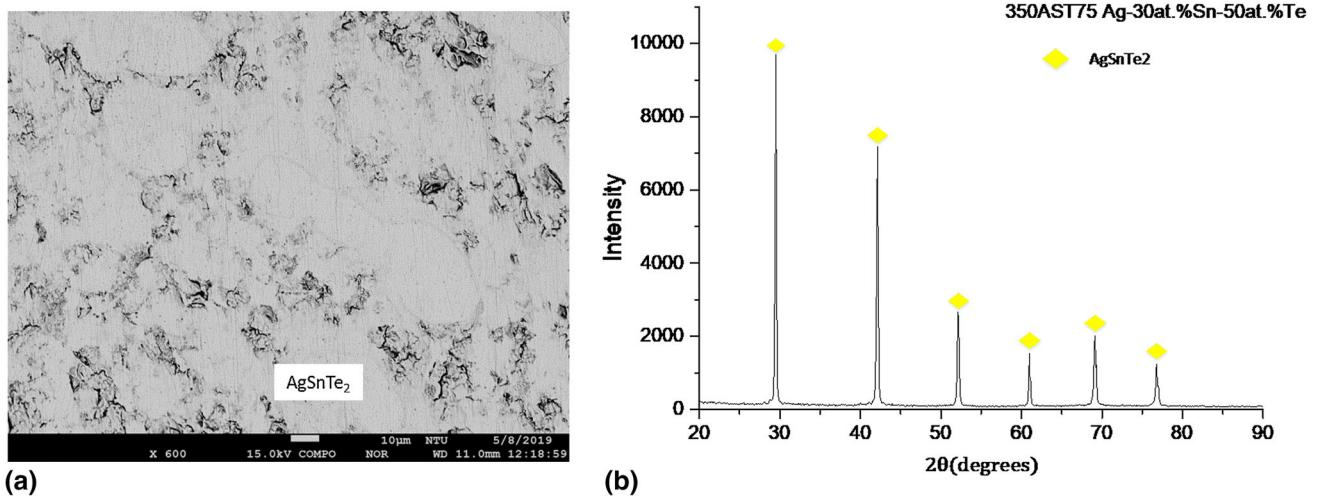
Fig. 5 Alloy #7 (Ag-35.0 at.% Sn-15.0 at.% Te) equilibrated at 350 °C (a) BEI micrograph (b) x-ray powder diffractogram

Fig. 6. Alloy #15 (Ag-85.0.at.%Sn-5.0.at.%Te) equilibrated at 350 °C (a) BEI micrograph (b) x-ray powder diffractogram

be approximately Ag-10.0 at.%Sn-70.0 at.%Te. This liquid phase is not connected with the Ag-Te binary phase diagram. The x-ray diffractogram is shown in Fig. 8(b). The results are consistent with the compositional analysis and alloy #35 should lie in the $Ag_xSn_{2-x}Te_2$+(Te)+Liquid three-phase field.

No experimental sample showed the Ag_5Te_3+Te+Liquid three-phase region.

3.1.8 Ag-Sn-Te Isothermal Section at 350 °C

The proposed Ag-Sn-Te isothermal section at 350 °C is shown in Fig. 9. Besides those binary compounds mentioned previously,[17–19] one ternary compound, $Ag_xSn_{2-x}Te_2$, exists at this temperature. Its composition was found to be slightly shifted towards higher Sn content (approx.

30 at.% Sn) in comparison with "ideal" composition ratio 1:1:2. A very similar composition of the ternary phase was found in all samples where this phase was found.

The isothermal section is designed based on the experimental results of this study, the results of phase equilibria studies in the literature[11-17] and theoretical calculations based on preliminary modeling using only parameters for binary subsystems. Eleven tie-triangles were observed in the Ag-Sn-Te ternary system at 350 °C, namely (Ag)+ζ-Ag_4Sn+β-Ag_2Te, ζ-Ag_4Sn+SnTe+β-Ag_2Te, ζ-Ag_4Sn+ε-Ag_3Sn+SnTe, ε-Ag_3Sn+Liquid+SnTe, $AgSnTe_2$+$-$SnTe+(Te), Ag_5Te_3+$AgSnTe_2$+Liquid, $AgSnTe_2$+Liquid+Te, Ag_5Te_3+Te+Liquid, β-Ag_2Te+$AgSnTe_2$+$Ag_{1.9}Te$, β-Ag_2Te+SnTe+$AgSnTe_2$, and $AgSnTe_2$+Ag_5Te_3+ $Ag_{1.9}Te$.

Fig. 7 Alloy #38 (Ag-30.0at.%Sn-50.0at.%Te) equilibrated at 350 °C (a) BEI micrograph (b) x-ray powder diffractogram
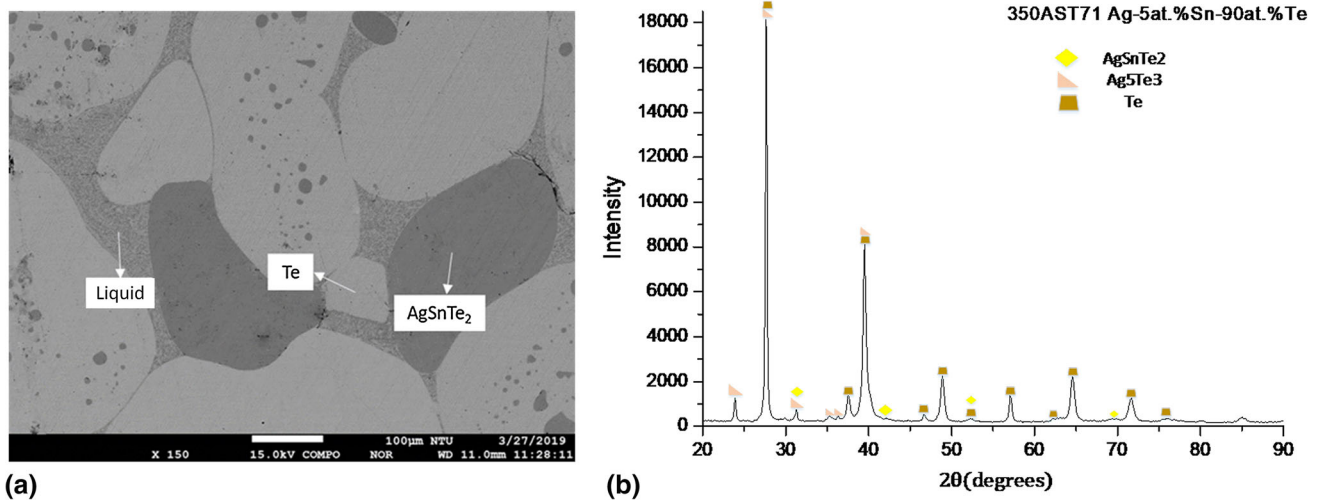

Fig. 8 Alloy #35 (Ag-5.0 at.% Sn-90.0 at.% Te) equilibrated at 350 °C (a) BEI micrograph (b) X-ray powder diffractogram

3.2 Ag-Sn-Te Isothermal Section at 500 °C

A total of 31 alloys were prepared for the isothermal section at 500 °C as shown in Fig. 10. Their nominal and determined compositions are shown in Table 2. All samples were annealed for 180 days at this temperature.

3.2.1 SnTe+Liquid

The BEI micrograph of alloy #56 (Ag-60.0 at.% Sn-30.0 at.% Te) is presented in Fig. 11(a). The analysis of the bright gray phase gives the composition Ag-51.2 at.% Sn-48.4 at.% Te, which corresponds well to the SnTe phase, while the dark gray phase is likely a liquid phase consisting of Sn and ε-Ag$_3$Sn phases after the decomposition during

cooling.[22,23] The x-ray diffraction pattern of alloy #56, where the peaks of SnTe, Sn and ε-Ag$_3$Sn phases were identified, is shown in Fig. 6(b). This alloy is in the SnTe+Liquid phase region. Similar results are found for alloys #39, 41, 46, 47, 57, 63, 64 and 65.

3.2.2 ζ-Ag$_4$Sn+SnTe+Liquid

The microstructure of alloy #66 (Ag-40.0 at.% Sn-10.0 at.% Te) is presented in Fig. 12(a). The composition of the large gray grains is Ag-50.1 at.% Sn-49.0 at.% Te and corresponds to the SnTe phase. The black phase composition is Ag-23.1 at.% Sn-0.2 at.% Te which agrees well with the presumed composition of the ζ-Ag$_4$Sn phase. The fine gray phase is too fine to be measured reliably,
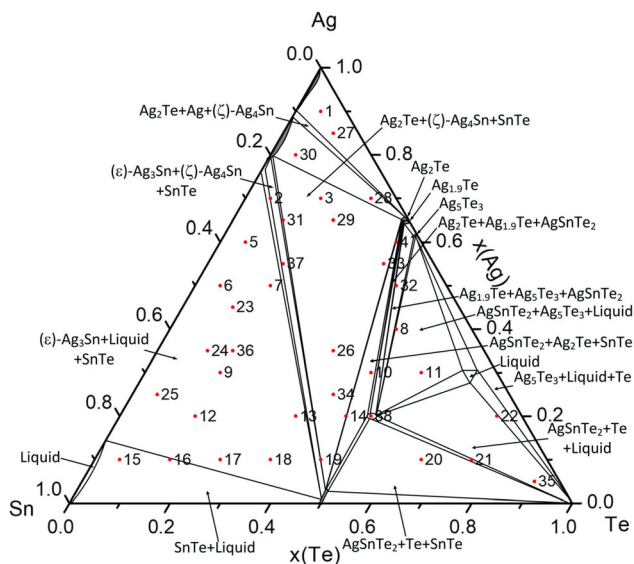
Fig. 9 The proposed Ag-Sn-Te isothermal section at 350 °C
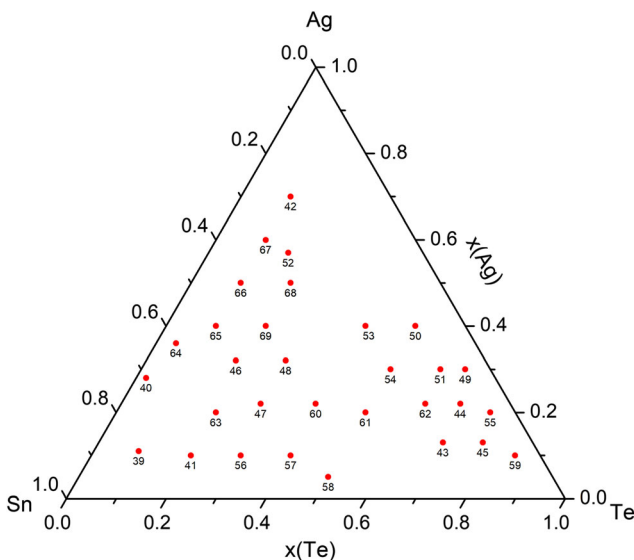

Fig. 10 Prepared and equilibrated alloys of Ag-Sn-Te at 500 °C for 180 days

however, the x-ray diffractogram of this alloy (Fig. 12b) shows the peaks of SnTe, ζ-Ag₄Sn, Sn, and ε-Ag₃Sn. These results indicate that this phase was liquid at 500 °C, consequently decomposing to of Sn and ε-Ag₃Sn phases.[22,23] Similar results were found for alloys #48, 67, and 69.

3.2.3 ζ-Ag₄Sn+SnTe+Ag₂Te

Figure 13(a) and (b) present the BEI micrograph and x-ray diffractogram of alloy #42 (Ag-20.0 at.%Sn-10.0 at.%Te), respectively. EPMA measurements show the composition

of the darkest phase as Ag-22.0 at.% Sn-1.7 at.% Te which corresponds well to the ζ-Ag4Sn phase, the light gray phase is SnTe with the composition of Ag-48.2 at.% Sn-49 , 0 at. % Te and the dark gray phase is β-Ag2Te with the composition of Ag-1.7 at.% Sn-34.5 at.% Te. Thus, the alloy #42 is in the ζ-Ag₄Sn+SnTe+β-Ag₂Te three-phase region. Similar results were also found for alloy #60.

3.2.4 Ag-Sn-Te Isothermal Section at 500 °C

The proposed isothermal section of the Ag-Sn-Te system at 500 °C is shown in Fig. 14. No ternary compound is observed. The result agrees with the previous literature results.[21] There are four tie-triangles, which are SnTe+Liquid+ζ-Ag₄Sn, ζ-Ag₄Sn+Ag+β-Ag₂Te, SnTe+ζ-Ag₄Sn+β-Ag₂Te, and SnTe+β-Ag₂Te+Liquid. There are eight two-phase regions: SnTe+Liquid (Sn), Liquid (Sn)+ζ-Ag₄Sn, ζ-Ag₄Sn+SnTe, Ag+β-Ag₂Te, ζ-Ag₄Sn+β-Ag₂Te, β-Ag₂Te+SnTe, β-Ag₂Te+Liquid (Te), and SnTe+Liquid (Te).

4 CALPHAD-type Modeling

A semi-empirical approach, referred to as the *CALPHAD* method[25,26] was used for thermodynamic modeling of the Ag-Sn-Te system and consequently, the relevant phase diagram sections and thermodynamic properties were calculated. The compositions of phases in equilibrium correspond to the minimum total Gibbs energy of a closed system at constant temperature and pressure. Calculations were done using Thermo-Calc[27] and Pandat[28] software packages which solve the constrained minimization problem to determine the set of nonnegative amounts of individual components in equilibrium phases. The Gibbs energies are considered relative to the Standard Element Reference state at 298.15K and 1 bar (SER).[29]

4.1 The Pure Elements

The Standard Element Reference (SER) states were chosen as standard states for pure solid elements and the corresponding temperature dependencies of Gibbs energies in stable and metastable structures were taken from the SGTE (Scientific Group Thermodata Europe) database, Version 5.0[30]

The temperature dependence of the Gibbs energy of the pure constituent i is expressed by the polynomial

$$G(T) = a + bT + cT\ln(T) + \sum_i d_i T^n \qquad \text{(Eq 1)}$$

where a, b, c, and the d_i are adjustable coefficients.

Table 2 Nominal composition and equilibrium phases of Ag-Sn-Te alloys equilibrated at 500 °C

Alloy no.	Nominal Composition (at.%)			Phase in equilibrium	Composition (at.%)		
	Ag	Sn	Te		Ag	Sn	Te
39	11	80	9	SnTe	0.8	49.4	49.8
				Liquid	…	…	…
40	28	70	2	Liquid	…	…	…
41	10	70	20	SnTe	0.6	49.6	49.8
				Liquid	…	…	…
42	70	20	10	Ag₄Sn	76.3	22.0	1.7
				Ag₂Te	63.8	1.7	34.5
				SnTe	2.8	48.2	49.0
43	13	18	69	Liquid	…	…	…
44	22	10	68	Liquid	…	…	…
45	13	10	77	Liquid	…	…	…
46	32	50	18	SnTe	0.3	50.8	48.9
				Liquid	…	…	…
47	22	50	28	SnTe	0.7	49.7	49.6
				Liquid	…	…	…
48	32	40	28	SnTe	0.7	49.4	49.9
				Ag₄Sn	76.63	22.74	0.63
				Liquid	…	…	…
49	30	5	65	Liquid	…	…	…
50	40	10	50	Liquid	…	…	…
51	30	10	60	Liquid	…	…	…
52	57	27	16	SnTe	2.0	47.6	50.4
				Ag₄Sn	77.3	21.8	0.9
53	40	20	40	SnTe	2.4	48.8	48.8
				Ag₂Te	62.3	0.7	37.0
54	30	20	50	SnTe	9.6	40.2	50.2
				Liquid	…	…	…
55	20	5	75	Liquid	…	…	…
56	10	60	30	SnTe	0.4	51.2	48.4
				Liquid	…	…	…
57	10	50	40	SnTe	0.7	49.6	49.7
				Liquid	…	…	…
58	5	45	50	SnTe	8.6	41.4	50.0
59	10	5	85	Liquid	…	…	…
60	22	39	39	SnTe	2.2	48.6	49.2
				Ag₂Te	64.2	2.4	33.4
				Ag₄Sn	77.0	21.2	1.8
61	20	30	50	SnTe	9.7	40.8	49.5
				Liquid	…	…	…
62	22	17	61	Liquid	…	…	…
63	20	60	20	SnTe	0.3	51.6	48.1
				Liquid	…	…	…
64	36	60	4	Liquid	…	…	…
				SnTe	…	…	…
65	40	50	10	SnTe	0.8	50.7	48.5
				Liquid	…	…	…
66	50	40	10	SnTe	0.9	50.1	49.0

J. Phase Equilib. Diffus. (2022) 43:139–163

149

Table 2 continued

Alloy no.	Nominal Composition (at.%)			Phase in equilibrium	Composition (at.%)		
	Ag	Sn	Te		Ag	Sn	Te
				Ag₄Sn	76.7	23.1	0.2
				Liquid	…	…	…
67	60	30	10	SnTe	1.3	48.1	50.6
				Ag₄Sn	77.8	21.9	0.3
				Liquid	…	…	…
68	50	30	20	SnTe	0.4	50.3	49.3
				Ag₄Sn	77.0	22.2	0.8
69	40	40	20	SnTe	0.3	50.4	49.3
				Ag₄Sn	74.0	24.8	1.2
				Liquid	…	…	…
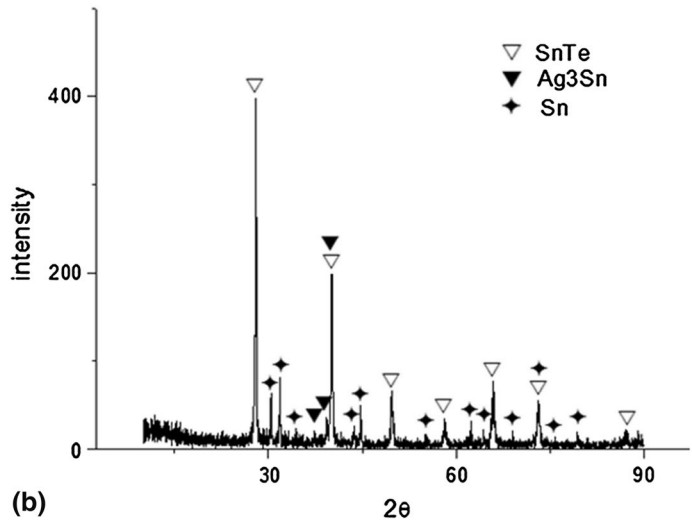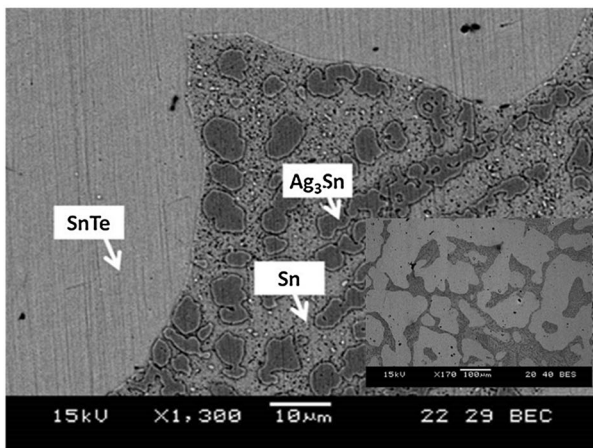
Fig. 11 Alloy #56 (Ag-60.0at.%Sn-30.0at.%Te) equilibrated at 500 °C (a) BEI micrograph (b) x-ray powder diffractogram
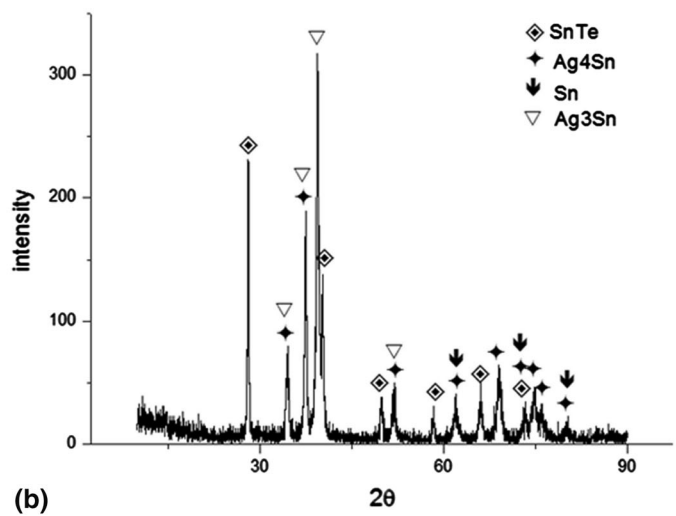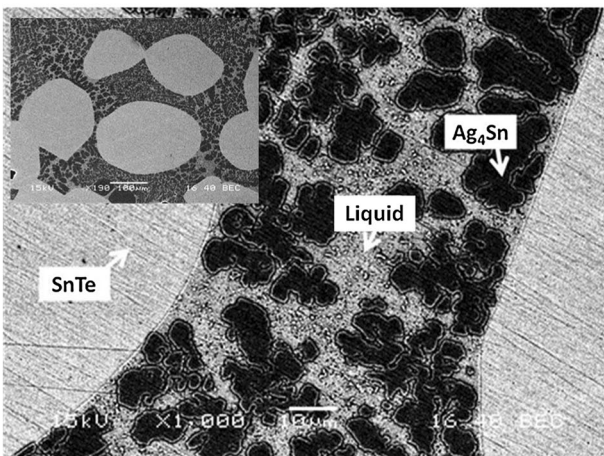
Fig. 12 Alloy #66 (Ag– 60.0at.%Sn-4.0at.%Te) equilibrated at 500 °C (a) BEI micrograph (b) x-ray powder diffractogram

150

J. Phase Equilib. Diffus. (2022) 43:139–163
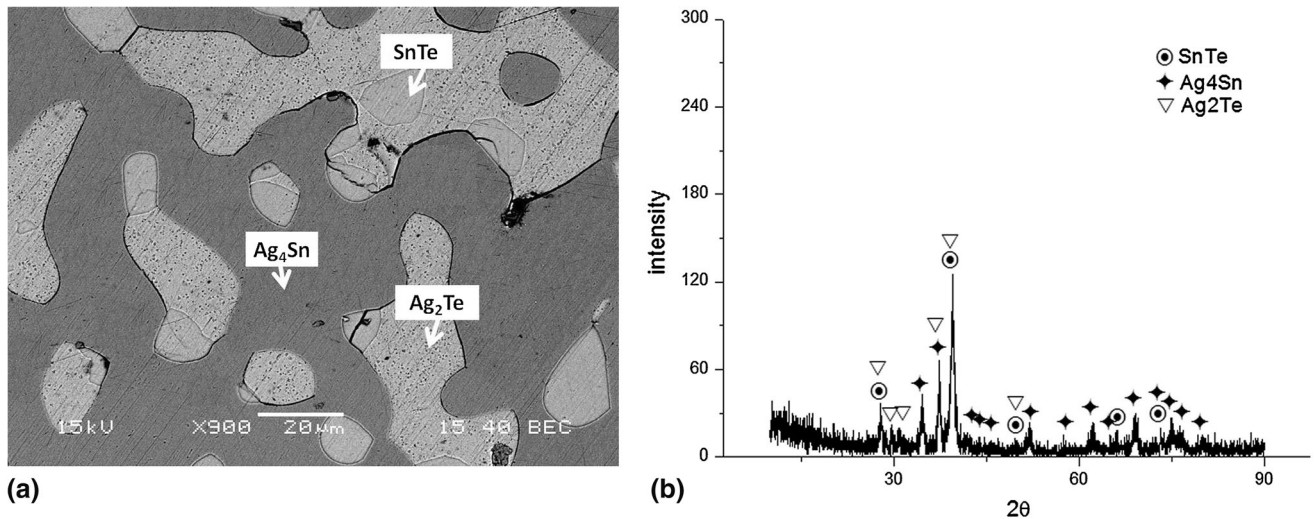
Fig. 13 Alloy #42 (Ag-20.0at.%Sn-10.0at.%Te) equilibrated at 500°C (a) BEI micrograph (b) x-ray powder diffractogram
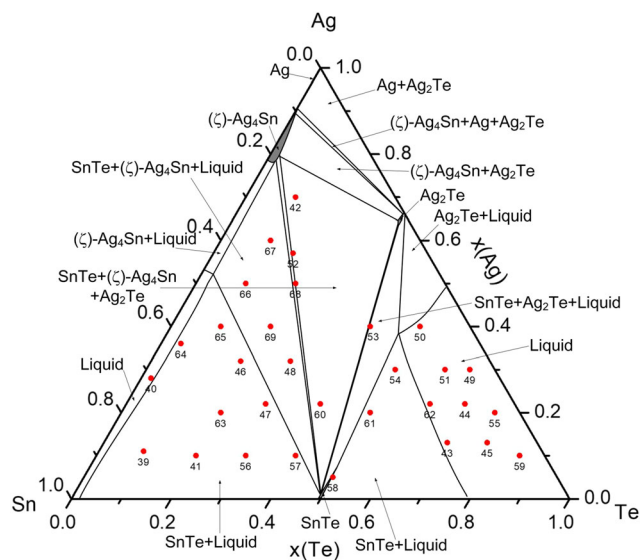
Fig. 14 The proposed Ag-Sn-Te isothermal section at 500 °C

4.2 The Solid Solution Phases

The Gibbs energies of the solid solution phases and liquid were modelled using a substitutional model with one sublattice. The molar Gibbs energy of the liquid (and solid solution generally) can be considered as the sum of several contributions:

$$G_m^{\varphi} = \sum_{i=1}^{n} x_i . G_i^{\varphi} + RT \sum_{i=1}^{n} x_i . \ln(x_i) + G_E^{\varphi} \qquad \text{(Eq 2)}$$

where the first term is the molar reference Gibbs energy which is the weighted sum of the Gibbs energies of the system constituents i in the crystallographic structure of the phase φ or in the liquid state relative to the chosen

reference state. The temperature dependence of the Gibbs energy of the pure constituent i is expressed by (Eq 1).

The second term of (Eq 2) is the contribution to the total Gibbs energy resulting from the ideal mixing of the constituents on the crystal lattice on in the liquid, where n is the number of constituents.

Third term, the excess Gibbs energy G_E^{φ}, describes the influence of the non-ideal behaviour of the system on the thermodynamic properties of the phase and is given by the Redlich–Kister–Muggianu formalism[31,32]

$$G_E^{\varphi} = \sum_{\substack{i,j=1 \\ i \neq j}}^{n} x_i x_j \sum_{z=0}^{m} {}^z L_{i,j} (x_i - x_j) + \sum_{1}^{n-2} \sum_{j=i+1}^{n-1} \sum_{k=j+1}^{n} x_i \cdot x_j$$
$$\cdot x_k \cdot L_{i,j,k} \qquad \text{(Eq 3)}$$

where ${}^z L_{i,j}$ are the temperature dependent binary interaction parameters, describing the mutual interaction between constituent i and j, and $L_{i,j,k}$ is the interaction parameter describing possible ternary interactions. Their temperature dependence is usually defined as:

$$L(T) = a + bT + cT\ln(T) \qquad \text{(Eq 4)}$$

The liquid, hex_A8 (Te), bct_A5 (Sn), and diam_A4 (α-Sn) phases were modeled using this model.

The fcc_A1 (Ag) and hcp_A3 (ζ-Ag₄Sn) phases can be modeled as substitutional solid solutions as well, but because it is advisable to retain consistency with models used in other databases, we used the two sublattice model for interstitial solid solution. More detailed description of this model, where one sublattice is used for elements occupying the substitutional positions in the crystallographic lattice (e.g., Ag, Sn, Te) and the second sublattice

is used for elements occupying the interstitial positions (e.g., C,N) and vacancies can be found e.g. in.[25,26] As the second sublattice for the interstitial elements is empty in this system, the resulting model is generally identical with the above-mentioned model for the substitutional solid solution.

As mentioned above the substitutional solid solution model was used to model solubilities of components in pure elements (hex_A8 (Te), bct_A5 (Sn), and diam_A4 (α-Sn)). In some cases, there is not enough information about solubilities of some components in other terminal solid solutions, or these solubilities are very low. This is true especially for tellurium. Therefore, the substitutional solid solution model for bct_A5 (Sn) was defined as (AG, SN)$_1$, and no solubility of other elements were considered for diam_A4 (Sn) and hex_A8 (Te).

The substitutional solution model with associates (AG, AG2TE, SN, SNTE, TE)$_1$ was used for the model of liquid phase with respect to the assessments of binary subsystems Ag-Te and Sn-Te.[22,24] This model is based on the formation of associates (AG2TE, SNTE) in the melts to account for abrupt changes in thermochemical quantities and phase diagrams.[26]

The fcc_A1 (Ag) phase was modelled using the interstitial solid solution model as (AG, SN)$_1$(VA)$_1$ with empty second sublattice. The interstitial model was also used for the ζ-Ag$_4$Sn intermetallic phase, which has hexagonal_A3 crystallographic structure. The model is described as (AG, SN, TE)$_1$(VA)$_{0.5}$. As in the case of fcc_A1 structure, the second sublattice is empty.

4.3 Intermetallic Phases

The intermetallic phases and the ternary phase were modelled using compound energy formalism (CEF) and the two-sublattice model was used in all cases. Only the basic principles of the CEF Gibbs energy modelling are shown here for the case of two sublattices. Details of this approach can be found in.[25,26]

The reference Gibbs energy equivalent to that in Eq 2 for such a model is given as:

$$G_{\text{ref}}^{\varphi} = \sum {}^1 y_i \cdot {}^2 y_j \cdot {}^0 G_{i:j}^{\varphi} \quad \text{i,j} = \text{Ag, Sn, Te} \qquad \text{(Eq 5)}$$

where the ${}^{p}y_{i(j)}$ terms are the site fractions of constituent i or j in the sublattices $p = 1, 2$ respectively. The term $G_{i:j}^{\varphi}$ describes the Gibbs energy of formation of the so-called "end member" $i:j$ (i,j = Ag, Sn, Te), or the Gibbs energy of pure element $i:i$ (i = Ag, Sn, Te) if all sublattices are occupied by the same component, in the crystallographic structure φ. Typically, only some of the end member compounds really exist, but Gibbs energy data for all end members are necessary for the modelling.

The ideal mixing term is given by

$$G_{id}^{\varphi} = \sum_{p=1}^{3} f_p \cdot \sum_{i=1}^{n} {}^{p} y_i \cdot \ln({}^{p} y_i) \qquad \text{(Eq 6)}$$

where f_p is the stoichiometric coefficient for sublattice p, and the second sum describes the effect of the ideal mixing within the sublattice p, similarly as in Eq 2.

The simplest model for the description of the contribution of the excess Gibbs energy is defined as:

$$G_E^{\varphi} = \sum {}^1 y_i \cdot {}^1 y_j \cdot {}^2 y_k \cdot L_{i,j:k} + \sum {}^1 y_k \cdot {}^2 y_i \cdot {}^2 y_j \cdot L_{k:i,j} \qquad \text{(Eq 7)}$$

where the parameters $L_{i,j:k}$ describe the mutual interaction of constituents i and j in the relevant sublattice, when the other sublattice is fully occupied by constituent k, similarly as in the (Eq 3).

The Ag-Sn contains two intermetallic phases. The ε-Ag$_3$Sn phase has an orthorhombic structure with the β-Cu$_3$Ti prototype. To retain consistency with other databases by unifying the models for phases with the same crystallographic structure, the intermetallic phase ε-Ag$_3$Sn was modeled by the two-sublattice model with the sublattice occupancy defined as (AG)$_3$(AG,SN,TE)$_1$. This phase was found to be almost stoichiometric in binary Ag-Sn system, but because of the above-mentioned consistency, the presence of Ag in the 2nd sublattice is needed. The name of the phase was selected to be CU3TI_TYPE in agreement with the convention adopted for the COST MP0602 Action database[33] The name for the family of phases with the same crystallographic structure is selected as the name of the prototype with the addition of the "_TYPE" suffix.

The model of the ζ-Ag$_4$Sn phase has the hcp structure and the interstitial solid solution model was used as described in the Sect. 4.2.

The Ag-Te system contains three intermetallic phase families, Ag$_2$Te, Ag$_{1.9}$Te and Ag$_5$Te$_3$. The Ag$_2$Te phase exists in three modifications. Low-temperature, monoclinic α-Ag$_2$Te form is stable up to 160 °C, intermediate, fcc-based β-Ag$_2$Te transforms to bcc-based γ-Ag$_2$Te at 695 °C. These polymorphic transformation temperatures apply when Ag$_2$Te has a slight excess of Te. The transformation temperatures when Ag$_2$Te has a slight excess of Ag are 160 °C for α↔β and 802 °C for β↔γ. The Ag$_2$Te family of phases were modeled by the two-sublattice models in agreement with relevant binary assessment.[24] The solubility of Sn in these phases is generally low and the models for α-Ag$_2$Te and β-Ag$_2$Te were defined as (AG,SN)$_{0.667}$(TE)$_{0.333}$. The γ-Ag$_2$Te phase has slightly different composition and the model is defined as (AG,SN)$_{0.666}$(TE)$_{0.334}$. The names AAG2TE, BAG2TE, GAG2TE were assigned to them in the thermodynamic dataset.

The $Ag_{1.9}Te$ phases exist within a narrow composition range (34.35 to 34.7 at. % Te) between 120 and 460 °C. Above this temperature it melts incongruently into Ag_2Te and liquid; below 120 °C it decomposes to Ag_2Te and Ag_5Te_3. A polymorphic $\alpha \leftrightarrow \beta$ transformation occurs near 180 °C, independent of composition. Similar to the case of Ag_2Te family of phases, the 2-sublattice models $(AG,SN)_{0.655}(TE)_{0.345}$ was used and the names AAG19TE, BAG19TE were assigned to them in the thermodynamic dataset.

The Ag_5Te_3 phase has been described variously as Ag_3Te_2, $Ag_{12}Te_7$, Ag_7Te_4 and as $Ag_{1.6}Te$ in the thermodynamic assessment of Gierlotka.[24] Two different crystallographic structures are thought to exist. Hexagonal α-Ag_5Te_3 transforms into the β form at 295 °C in the presence of excess Te.[34] The crystal structure of the β polymorph has not yet been identified. The Ag_5Te_3 family of phases was modeled similarly to other Ag-Te intermetallic phases by the two-sublattice model $(AG,SN)_{0.62}(TE)_{0.38}$. The names AAG16TE, BAG16TE were assigned to them in the thermodynamic dataset.

The Sn-Te system contains one intermetallic phase, SnTe. Tin telluride has a NaCl-type structure with the space group of $Fm\overline{3}m$. The homogeneity range of SnTe phase is shifted beyond the stoichiometric composition toward the Te-rich side. The SnTe phase was modeled by the two-sublattice model with the sublattice occupancy defined as $(AG,SN,VA)_1(TE)_1$.

The existence of the $Ag_xSn_{2-x}Te_2$ ternary phase in the Ag-Sn-Te system was confirmed in.[16,19] This phase has cubic crystallographic structure $cF8$ with NaCl prototype. The model for this phase was selected with respect to the crystallography as $(AG,SN)_{0.5}(TE)_{0.5}$.

4.4 The Binary Systems

The binary data of constituting subsystems are used for ternary extrapolation of Ag-Sn-Te system and consequently for the creation of its full assessment. The prediction gives us basic knowledge of the phase equilibria in the system but usually does not offer information on the solubility of the third element in binary phases and no prediction of any ternary phase is possible.

The basic thermodynamic dataset for Ag-Sn system was taken from.[23] The data for the FCC_A1 (Ag) phase has been remodeled within the scope of the COST 531 Action to be compatible with the adopted data for lattice stability of FCC_A1 (Sn) from the SGTE database for unary elements.[30] Also, the Gibbs energy expression of the liquid phase was re-optimized by Watson[35] using the enthalpy of mixing data from Flandorfer et al.[36] in addition to the

other experimental data compiled by Chevalier.[37] The calculated Ag-Sn phase diagram is presented in Fig. 15.

The dataset for Ag-Te system is taken from the assessments done by Gierlotka.[24] The dataset used in this paper is based on previous work of Gierlotka,[38] where he assessed the Ag-Te phase diagram including the polymorphic variations of intermetallic phases based on comprehensive overview of experimental results. He used both solution model with associates and ionic liquid model for the description of the liquid phase and the dataset with ionic liquid model was published in.[38] The dataset using associate model for liquid phase was taken from Ref.[24] and parameters are presented in Table 3.

The Ag-Te system consists of 6 phases, liquid with a miscibility gap, fcc (Ag), hexagonal (Te), Ag_2Te, $Ag_{1.9}Te$ and Ag_5Te_3. The substitutional model for liquid with AG2TE associate was used in the assessment. The calculated Ag-Te phase diagram is shown in Fig. 16.

The dataset for Sn-Te system was taken from Liu et al.[22] The Sn-Te binary phase diagram is relatively simple, only one congruently melting intermediate phase exists and two eutectic reactions are observed. The solution model with associate is again utilized to describe the thermodynamic properties of liquids in the Sn-Te system in.[22] According to this model, the Sn-Te melt consists of three species, SN, SNTE, and TE. Figure 17 shows the calculated Sn-Te phase diagram. The thermodynamic parameters for all binary subsystems are summarized in Table 3.
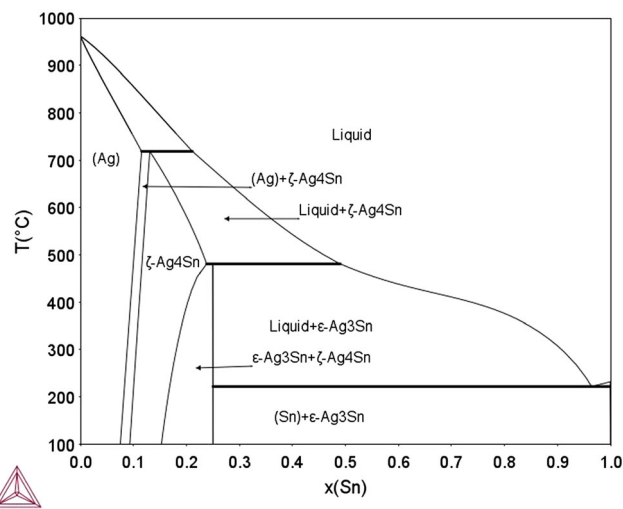

Fig. 15 The Ag-Sn phase diagram calculated with the data from the Table 3

Table 3 Thermodynamic parameters for the Ag-Sn-Te system

Database name (constituents) Thermodynamic parameters	Common Name	Lit.
GHSERAG = (298.15K $< T <$ 1234.93K): $- 7209.512$ $+118.202013 \cdot T - 23.8463314 \cdot T \cdot \ln(T) - 0.001790585 \cdot T^2 - 3.98587 \cdot 10^{-7} \cdot T^3 - 12011 \cdot T^{-1}$ (1234.93K $< T <$ 3000K): $- 15095.252$ $+190.266404 \cdot T - 33.472 \cdot T \cdot \ln(T) + 1.411773 \cdot 10^{29} \cdot T^{-9}$	Ag	30
GHSERSN = (100K $< T <$ 250K): $- 7958.517 + 122.765451 \cdot T - 25.858 \cdot T \cdot \ln(T) + 5.1185E - 04 \cdot T^2 - 3.192767 \cdot 10^{-6} \cdot T^3 + 18440 \cdot T^{-1}$ (250K $< T <$ 505.08K): $- 5855.135$ $+65.443315 \cdot T - 15.961 \cdot T \cdot \ln(T) - 0.0188702 \cdot T^2 + 3.121167 \cdot 10^{-6} \cdot T^3$ $- 61960 \cdot T^{-1}$ (505.08K $< T <$ 800K): $+2524.724 + 4.005269 \cdot T - 8.2590486 \cdot T \cdot \ln(T) - 0.016814429 \cdot T^2$ $+2.623131 \cdot 10^{-6} \cdot T^3 - 1081244 \cdot T^{-1} - 1.2307 \cdot 10^{25} \cdot T^{-9}$ (800K $< T <$ 3000K): $- 8256.959 + 138.99688*T - 28.4512 \cdot T \cdot \ln(T) - 1.2307 \cdot 10^{25} \cdot T^{-9}$	β-Sn	30
GHSERTE = (298.15K $< T <$ 722.66 K): $- 10544.679 + 183.372894 \cdot T - 35.6687 \cdot T \cdot \ln(T) + .01583435 \cdot T^2 - 5.240417 \cdot 10^{-6} \cdot T^3 + 155015 \cdot T^{-1}$ (722.66K $< T <$ 1150K): $+9160.595 - 129.265373 \cdot T + 13.004 \cdot T \cdot \ln(T) - .0362361 \cdot T^2 + 5.006367 \cdot 10^{-6} \cdot T^3 - 1286810 \, T^{-1}$ (1150K $< T <$ 1600K): $- 12781.349 + 174.901226 \cdot T - 32.5596 \cdot T \cdot \ln(T)$	Te	30
Liquid phase: (Ag, Ag2Te, Sn, SnTe, Te)		
G_{Ag}^{LIQ} = (298.15K $< T <$ 1234.93K): $+3815.564 + 109.310993 \cdot T$ $- 23.8463314 \cdot T \cdot \ln(T) - 0.001790585 \cdot T^2 - 3.98587 \cdot 10^{-7} \cdot T^3$ $- 12011 \cdot T^{-1} - 1.033905 \cdot 10^{-20} \cdot T^7$ (1234.93K $< T <$ 3000K): $- 3587.111 + 180.964656 \cdot T - 33.472 \cdot T \cdot \ln(T)$	Liquid	30
G_{Sn}^{LIQ} = (100K $< T <$ 250K): $- 855.425$ $+108.677684 \cdot T - 25.858 \cdot T \cdot \ln(T)$ $+5.1185E - 04 \cdot T^2 - 3.192767 \times 10^{-6} T^3 + 18440 \cdot T^{-1}$ $+1.47031 \cdot 10^{-18} T^7$ (250K $< T <$ 505.08K): $+1247.957 + 51.355548 \cdot T - 15.961 \cdot T \cdot \ln(T)$ $- 0.0188702 \cdot T^2 + 3.121167 \cdot 10^{-6} T^3 - 61960 \cdot T^{-1} + 1.47031 \cdot 10^{-18} \cdot T^7$ (505.08K $< T <$ 800K): $+9496.31 - 9.809114 \cdot T$ $- 8.2590486 \cdot T \cdot \ln(T) - 0.016814429 \cdot T^2 + 2.623131 \cdot 10^{-6} \cdot T^3$ $- 1081244 \cdot T^{-1}$ (800K $< T <$ 3000K): $- 1285.372 + 125.182498 \cdot T - 28.4512 \cdot T \ln \cdot (T)$		30
G_{Te}^{LIQ} = (298.15K $<$ T $<$ 626.49K): $- 17554.731 + 685.877639 \cdot T$ $- 126.318 \cdot T \cdot \ln(T) + 0.2219435 \cdot T^2 - 9.42075 \cdot 10^{-5} \cdot T^3$ $+827930 \cdot T^{-1}$ (626.49K $<$ T $<$ 722.66K): $- 3165763.48 + 46756.357 \cdot T$ $- 7196.41 \cdot T \cdot \ln(T) + 7.09775 \cdot T^2 - 0.00130692833 \cdot T^3$ $+2.58051 \cdot 10^8 \cdot T^{-1}$ (722.66K $<$ T $<$ 1150K): $+180326.959 - 1500.57909 \cdot T$ $+202.743 \cdot T \cdot \ln(T) - 0.142016 \cdot T^2 + 1.6129733 \cdot 10^{-5} T^3 - 24238450 \cdot T^{-1}$ (1150K $<$ T $<$ 1600K): $+6328.687 + 148.708299 T$ $- 32.5596 \cdot T \cdot \ln(T)$		30
$^0G^{LIQ}_{Ag2Te} = - 20686.709 - 45.267329 \cdot T + GHSERTE + 2*GHSERAG$		24
$^0G^{LIQ}_{SnTe} = +GLIQSN + GLIQTE - 53949.9 + 10.88 \cdot T$		24
$^0L^{LIQ}_{Ag,Sn} = - 3177.49 - 10.16124 \cdot T + 0.380505 \cdot T \cdot \ln(T)$		33
$^1L^{LIQ}_{Ag,Sn} = - 16782.28 + 2.06521 \cdot T + 0.437477 \cdot T \cdot \ln(T)$		33
$^2L^{LIQ}_{Ag,Sn} = +3190.34 - 107.09456 \cdot T + 13.954838 \cdot T \cdot \ln(T)$		33

154

J. Phase Equilib. Diffus. (2022) 43:139–163

Table 3 continued

Database name (constituents) Thermodynamic parameters	Common Name	Lit.
$^0L^{LIQ}_{Ag,Ag2Te} = +27135.765 - 2.6400871 \cdot T$		24
$^0L^{LIQ}_{Ag2Te,Te} = +304.2709 - 4.0931618 \cdot T$		24
$^1L^{LIQ}_{Ag2Te,Te} = +2825.7135 - 0.48019091 \cdot T$		24
$^0L^{LIQ}_{Sn,SnTe} = +18582.149 - 6.01 \cdot T$		22
$^1L^{LIQ}_{Sn,SnTe} = +4263.6 - 1.98 \cdot T$		22
$^0L^{LIQ}_{SnTe,Te} = -3804.7$		22
$^0L^{LIQ}_{Ag,Ag2Te,SnTe} = -30000$		[*]
$^1L^{LIQ}_{Ag,Ag2Te,SnTe} = 0$		[*]
$^2L^{LIQ}_{Ag,Ag2Te,SnTe} = -17444 + 28 \cdot T$		[*]
$^0L^{LIQ}_{Ag2Te,Sn,SnTe} = 0$		[*]
$^1L^{LIQ}_{Ag2Te,Sn,SnTe} = 60000$		[*]
$^2L^{LIQ}_{Ag2Te,Sn,SnTe} = 0$		[*]
$^0L^{LIQ}_{Ag,Ag2Te,Sn} = 15000$		[*]
$^1L^{LIQ}_{Ag,Ag2Te,Sn} = 0$		[*]
$^2L^{LIQ}_{Ag,Ag2Te,Sn} = 45000$		[*]
$^0L^{LIQ}_{Ag2Te,SnTe,Te} = -30000$		[*]
$^1L^{LIQ}_{Ag2Te,SnTe,Te} = -80000$		[*]
$^2L^{LIQ}_{Ag2Te,SnTe,Te} = -130000$		[*]
$^0L^{LIQ}_{Ag,Sn,SnTe} = 0$		[*]
$^1L^{LIQ}_{Ag,Sn,SnTe} = 40000$		[*]
$^2L^{LIQ}_{Ag,Sn,SnTe} = -30000$		[*]
$^0L^{LIQ}_{Ag2Te,SnTe} = 24968 - 36 \cdot T$		[*]
$^1L^{LIQ}_{Ag2Te,SnTe} = -2095 + 15 \cdot T$		[*]
$^2L^{LIQ}_{Ag2Te,SnTe} = -13000 + 10 \cdot T$		[*]
FCC_A1 phase: (Ag, Sn)$_1$(Va)$_1$	(Ag)	
$^0G^{FCC\_A1}_{Ag:Va} = (298.15K < T < 1234.93K): -7209.512 + 118.202013 \cdot T$		30
$\quad -23.8463314 \cdot T \cdot \ln(T)$		
$\quad -0.001790585 \cdot T^2 - 3.98587 \cdot 10^{-6} \cdot T^3$		
$\quad -12011 \cdot T^{-1}$		
$\quad (1234.93K < T < 3000K): -15095.252 + 190.266404 \cdot T$		
$\quad -33.472 \cdot T \cdot \ln(T) + 1.411773 \cdot 10^{29} \cdot T^{-9}$		
$^0G^{FCC\_A1}_{Sn:Va} = (298.15K < T < 505.08K): -345.135$		22
$\quad +56.983315 \cdot T - 15.961 \cdot T \cdot \ln(T) - 0.0188702 \cdot T^2 + 3.121167 \cdot 10^{-6} \cdot T^3 - 61960 \cdot T^{-1}$		
$\quad (505.08K < T < 800K): +8034.724 - 4.454731 \cdot T$		
$\quad -8.2590486 \cdot T \cdot \ln(T) - 0.016814429 T^2 + 2.623131 \times 10^{-6} T^3$		
$\quad -1081244 T^{-1} - 1.2307 \cdot 10^{25} \cdot T^{-9}$		
$\quad (800K < T < 3000K): -2746.959 + 130.53688 \cdot T - 28.4512 \cdot T \cdot \ln(T)$		
$\quad -1.2307 \cdot 10^{25} \cdot T^{-9}$		
$^0L^{FCC\_A1}_{Ag,Sn:Va} = +745.45 + 11.498027 \cdot T$		22
$^1L^{FCC\_A1}_{Ag,Sn:Va} = -36541.5$		22
HCP_A3 phase: (Ag, Sn, Te)$_1$(Va)$_{0.5}$	ζ-Ag$_4$Sn	
$^0G^{HCP\_A3}_{Ag:Va} = (298.15K < T < 1234.93K): -6909.512 + 118.502013 \cdot T$		22
$\quad -23.8463314 \cdot T \cdot \ln(T) - .001790585 \cdot T^2 - 3.98587 \cdot 10^{-7} \cdot T^3 - 12011 \cdot T^{-1}$		
$\quad (1234.93K < T < 3000K): -14795.252 + 190.566404 \cdot T$		
$\quad -33.472 \cdot T \cdot \ln(T) + 1.411773 \cdot 10^{29} \cdot T^{-9}$		

Table 3 continued

Database name (constituents) Thermodynamic parameters	Common Name	Lit.
$^0G^{HCP\_A3}_{Sn:Va} = (298.15K < T < 505.08K): -1955.135 +57.797315 \cdot T$		22
$-15.961 \cdot T \cdot \ln(T) - 0.0188702 \cdot T^2 +3.121167 \cdot 10^{-6} \cdot T^3 - 61960 \cdot T^{-1}$		
$(298.15K < T < 800K): +6424.724 - 3.640731 \cdot T$		
$-8.2590486 \cdot T \cdot \ln(T) - 0.016814429 \cdot T^2 +2.623131 \cdot 10^{-6} \cdot T^3$		
$-1081244 \cdot T^{-1} - 1.2307 \cdot 10^{25} \cdot T^{-9}$		
$(800K < T < 3000K): -4356.959 +131.35088 \cdot T - 28.4512 \cdot T \cdot \ln(T)$		
$-1.2307 \cdot 10^{25} \cdot T^{-9}$		
$^0G^{HCP\_A3}_{Te:Va} = +5000 + GHSERTE$		[*]
$^0L^{HCP\_A3}_{Ag,Sn:Va} = +1046.1 +10.23693 \cdot T$		22
$^1L^{HCP\_A3}_{Ag,Sn:Va} = -40505.5$		22
$^0L^{HCP\_A3}_{Ag,Sn,Te:Va} = -459000$		[*]
$^1L^{HCP\_A3}_{Ag,Sn,Te:Va} = 489000$		[*]
$^2L^{HCP\_A3}_{Ag,Sn,Te:Va} = 450000$		[*]
BCT_A5 phase: (Ag, Sn)$_1$	β-Sn	
$^0G^{BCT\_A5}_{Ag} = (298.15K < T < 1234.93K): -3025.412 +118.202013 \cdot T$		22
$-23.8463314 \cdot T \cdot \ln(T) - 0.001790585 \cdot T^2 - 3.98587 \cdot 10^{-7} \cdot T^3$		
$-12011 \cdot T^{-1}$		
$(1234.93K < T < 3000K): -10911.152 +190.266404 \cdot T$		
$-33.472 \cdot T \cdot \ln(T) +1.411773 \cdot 10^{29} \cdot T^{-9}$		
$^0G^{BCT\_A5}_{Sn} = (100K < T < 250K): -7958.517 +122.765451 \cdot T$		30
$-25.858 \cdot T \cdot \ln(T) +5.1185 \cdot 10^{-4} \cdot T^2 - 3.192767 \cdot 10^{-6} \cdot T^3 +18440 \cdot T^{-1}$		
$(250K < T < 505.08K): -5855.135 +65.443315 \cdot T - 15.961 \cdot T \cdot \ln(T)$		
$-0.0188702 \cdot T^2 +3.121167 \cdot 10^{-6} \cdot T^3 - 61960 \cdot T^{-1}$		
$(505.08K < T < 800K): +2524.724 +4.005269 \cdot T$		
$-8.2590486 \cdot T \cdot \ln(T) - 0.016814429 \cdot T^2 +2.623131 \cdot 10^{-6} \cdot T^3$		
$-1081244 \cdot T^{-1} - 1.2307 \cdot 10^{25} \cdot T^{-9}$		
$(800K < T < 3000K): -8256.959 +138.99688 \cdot T$		
$-28.4512 \cdot T \cdot \ln(T) - 1.2307 \cdot 10^{25} \cdot T^{-9}$		
$^0L^{BCT\_A5}_{Ag,Sn} = +18358.8$		22
DIAMOND_A4 phase: (Sn)$_1$	(α-Sn)	
$^0G^{Diamond\_A4}_{Sn} = (100K < T < 298.15K): -9579.608 +114.007785 \cdot T$		30
$-22.972 \cdot T \cdot \ln(T) - 0.00813975 \cdot T^2 +2.7288 \cdot 10^{-6} \cdot T^3 +25615 \cdot T^{-1}$		
$(298.15K < T < 800K): -9063.001 +104.84654 \cdot T$		
$-21.5750771 \cdot T \cdot \ln(T) - 0.008575282 \cdot T^2 +1.784447 \cdot 10^{-6} \cdot T^3$		
$-2544 \cdot T^{-1}$		
$(800K < T < 3000K): -10909.351 +147.396535 \cdot T$		
$-28.4512 \cdot T \cdot \ln(T)$		
CU3TI_TYPE phase: (Ag)$_3$(Ag,Sn,Te)$_1$	ε-Ag$_3$Sn	
FUNCTION GAG3SN = $(298.15K < T < 6000K): -11085.3$		23
$+110.01471 \cdot T - 23.18 \cdot T \cdot \ln(T) - 0.00359 \cdot T^2 +4389.5 \cdot T^{-1}$		
$^0G^{CU3TI\_TYPE}_{Ag:Ag} = 4*GHSERAG + 20000$		23
$^0G^{CU3TI\_TYPE}_{Ag:Sn} = 4*GAG3SN$		23
$^0G^{CU3TI\_TYPE}_{Ag:Te} = 3*GHSERAG + GHSERTE + 20000$		[*]
$^0L^{CU3TI\_TYPE}_{Ag:Sn,Te} = -43466.67 - 66.6667 \cdot T$		[*]
$^1L^{CU3TI\_TYPE}_{Ag:Sn,Te} = 8000$		[*]
$^2L^{CU3TI\_TYPE}_{Ag:Sn,Te} = -16991.90 +35.3 \cdot T$		[*]
SNTE phase: (Ag, Sn, Va)$_1$ (Te)$_1$	SnTe	
$^0G^{SNTE}_{Sn:Te} = +GHSERSN + GHSERTE - 60127.5 - 0.305 \cdot T$		22

156

J. Phase Equilib. Diffus. (2022) 43:139–163

Table 3 continued

| Database name (constituents) Thermodynamic parameters	Common Name	Lit.
$^0G^{SNTE}_{Va:Te} = +GHSERTE+10000$		[*]
$^0G^{SNTE}_{Ag:Te} = GHSERAG+GHSERTE+10000$		[*]
$^0L^{SNTE}_{Sn,Va:Te} = +9503.72+10.51 \cdot T$		22
$^1L^{SNTE}_{Sn,Va:Te} = +23057.42- 45.03 \cdot T$		22
$^0L^{SNTE}_{Ag,Sn:Te} = - 68676.25+21.75 \cdot T$		[*]
$^1L^{SNTE}_{Ag,Sn:Te} = - 10290+40*T$		[*]
$^2L^{SNTE}_{Ag,Sn:Te} = 10290-40*T$		[*]
HEX_A8 phase: (Te)$_1$	Hexagonal_A8	
$^0G^{HEX\_A8}_{Te} = GHSERTE$		30
AAG16TE phase: (Ag,Sn)$_{0.62}$(Te)$_{0.38}$	α-Ag$_5$Te$_3$	
$^0G^{AAG16TE}_{Ag:Te} = +0.62*GHSERAG +0.38*GHSERTE - 18649.483 +1.8425 \cdot T$		24
$^0G^{AAG16TE}_{Sn:Te} =+0.62*GHSERSN+0.38*GHSERTE+5000$		[*]
BAG16TE phase: (Ag,Sn)$_{0.62}$(Te)$_{0.38}$	β- Ag$_5$Te$_3$	
$^0G^{BAG16TE}_{Ag:Te} = +0.62*GHSERAG +0.38*GHSERTE - 14800.208$ $- 4.933 \cdot T$		24
$^0G^{BAG16TE}_{Sn:Te} = +0.62*GHSERSN+0.38*GHSERTE+5000$		[*]
$^0L^{BAG16TE}_{Ag,Sn:Te} = - 10000$		[*]
AAG19TE phase: (Ag,Sn)$_{0.655}$(Te)$_{0.345}$	α-Ag$_{1.9}$Te	
$^0G^{AAG19TE}_{Ag:Te} = +0.655*GHSERAG +0.345*GHSERTE - 15313.327$ $- 3.3524 \cdot T$		24
BAG19TE phase: (Ag,Sn)$_{0.655}$(Te)$_{0.345}$	β-Ag$_{1.9}$Te	
$^0G^{BAG19TE}_{Ag:Te} = +0.655*GHSERAG +0.345*GHSERTE - 12593.224$ $- 9.3501 \cdot T$		24
$^0G^{BAG19TE}_{Sn:Te} = +0.655*GHSERSN+0.345*GHSERTE+5000$		[*]
AAG2TE phase: (Ag,Sn)$_{0.667}$(Te)$_{0.333}$	α-Ag$_2$Te	
$^0G^{AAG2TE}_{Ag:Te} = +0.667*GHSERAG +0.333*GHSERTE- 15605.8216$ $- 1.5 \cdot T$		24
$^0G^{AAG2TE}_{Sn:Te} = +0.667*GHSERSN+0.333*GHSERTE+5000$		[*]
$^0L^{AAG2TE}_{Ag,Sn:Te} = - 8000$		[*]
BAG2TE phase: (Ag, Sn)$_{0.667}$(Te)$_{0.333}$	β-Ag$_2$Te	
$^0G^{BAG2TE}_{Ag:Te} = +0.667*GHSERAG +0.333*GHSERTE - 11219.667$ $- 11.6251 \cdot T$		24
$^0G^{BAG2TE}_{Sn:Te} = +0.667*GHSERSN+0.333*GHSERTE+5000$		[*]
$^0L^{BAG2TE}_{Ag,Sn:Te} = 7866.39- 32.8879 \cdot T$		[*]
GAG2TE phase: (Ag, Sn)$_{0.666}$(Te)$_{0.334}$	γ-Ag$_2$Te	
$^0G^{GAG2TE}_{Ag:Te} = +0.666*GHSERAG +0.334*GHSERTE$ $- 10502.674- 12.3584 \cdot T$		24
$^0G^{GAG2TE}_{Sn:Te} = +0.666*GHSERAG+0.334*GHSERTE+5000$		[*]
$^0L^{GAG2TE}_{Ag,Sn:Te} = 3990.56- 33.635 \cdot T$		[*]
AGSNTE2 phase: (Ag,Sn)$_{0.5}$(Te)$_{0.5}$	Ag$_x$Sn$_{2- x}$Te$_2$	
$^0G^{AGSNTE2}_{Ag:Te} = +0.5*GHSERAG+0.5*GHSERTE +5000$		[*]
$^0G^{AGSNTE2}_{Sn:Te} = +0.5*GHSERSN+0.5*GHSERTE- 5000$		[*]
$^0L^{AGSNTE2}_{Ag,Sn:Te} = - 107447.4+28.407 \cdot T$		[*]
$^1L^{AGSNTE2}_{Ag,Sn:Te} = 60000$		[*]

*parameters optimized in this work
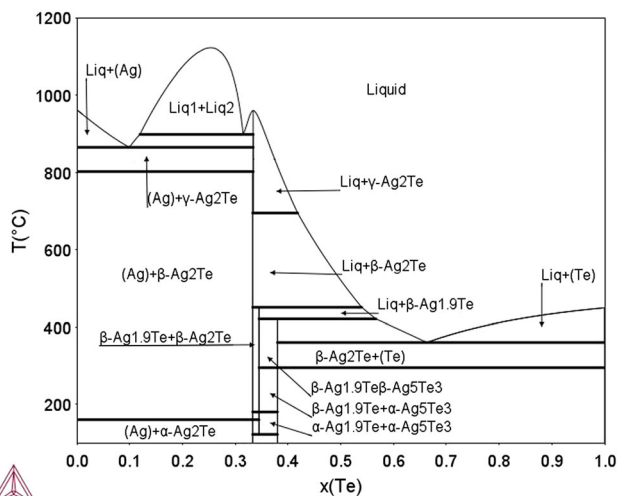
Fig. 16 The Ag-Te phase diagram calculated with the data from the Table 3
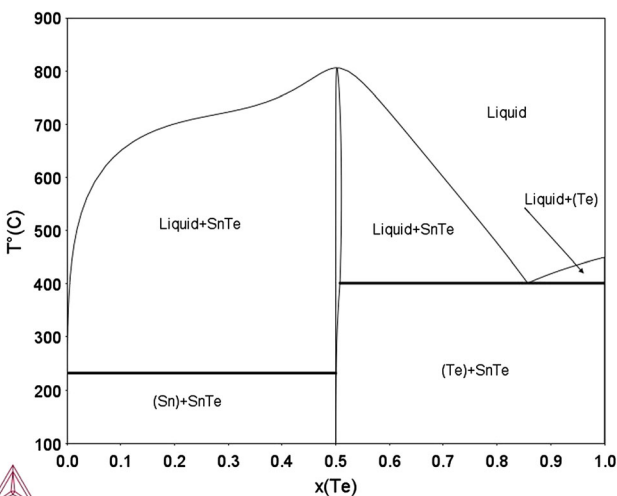

Fig. 17 The Sn-Te phase diagram calculated with the data from the Table 3

5 Theoretical Results

Our own experimental results and results from literature were used for the theoretical assessment of the Ag-Sn-Te system, using the Thermo-Calc and PANDAT software packages. In the case of the phase data, two experimental isothermal sections for 350 and 500 °C were obtained in the scope of this work (Fig. 9 and 14) and set of isopleths were presented in the paper from Blachnik et al.[16] The error bars were given for the invariant reactions (IR) in[16] where the vertical sections of the Ag-Sn-Te system were studied by the means of DTA analysis, and these values are shown in Table 4 for the shown IR. The error bars of IR without liquid phase are similar in size. Nevertheless,

Blachnik et al.[16] did not present any detailed information how they established the error bars in their paper.

The liquidus projection of the Ag-Sn-Te system was studied in Blachnik et al.[16] and Chang et al.[18] There is good agreement between results presented in these two papers and the data from Chang et al.[18] were used in the assessment.

In the case of thermodynamic data, the enthalpies of mixing in liquid for x(Ag)/x(Sn) ratio 0.78/0.22, 0.59/0.41, 0.40/0.60 and 0.20/0.80 at 887 °C were presented by Gather and Blachnik.[20] Römermann and Blachnik published the enthalpies of mixing for x(Ag)/x(Sn)=1 at 700, 800 and 900 °C in.[21] The information of experimental uncertainties for the enthalpies of mixing in liquid published in[20,21] is also very brief. The authors just published the reproducibility of the calibration measurements. No further information is available. These values are generally not acceptable for the evaluation of the experimental errors for real measurements, as the scattering of measured enthalpies is much higher than above mentioned values. Therefore, the estimation of any reasonable error bars for this experimental data is not possible.

In addition, there is inconsistency between the experimental datasets from[20] and.[21] Generally, the agreement between the experimental data for all 4 Ag/Sn ratios at 887 °C and the calculated curves is very good and has the same character for all Ag/Sn ratios. It was found during the assessment process that the agreement between experimental data from[21] and preliminary calculations are significantly worse especially close to the binary Ag-Sn side. Therefore, only the experimental data from[20] were used during the assessment process and the data from[21] were only compared with the calculated curves from the final database.

Above listed experimental datasets were used for the assessment together with binary assessments.[22–24] The assessed theoretical dataset is presented in the Table 3.

The results of the assessment are presented in this section of the paper. The isothermal sections at 350 and 500 °C are shown in Fig. 18, 19. The calculations are compared with the experimental results presented in the experimental part of this paper. The calculated isopleths for 10 at.% Sn, 10 at.% Te, 30 at.% Ag and for the Ag$_2$Te-Sn vertical section are shown in Fig. 20, 21, 22 and 23. Again, the results are compared with the experimental results from the thermal analysis presented in the paper.[16]

The thermodynamic properties, namely the enthalpies of mixing in liquid, were also calculated and compared with existing experimental data published by Gather and Blachnik[20] and Römermann and Blachnik[21] The representative sections are shown in Fig. 24, 25, 26 and 27.

The experimental study of liquidus surface was carried by Blachnik et al. in the scope of his work[16] and later by

Table 4 Invariant reactions in Ag-Sn-Te system containing liquid phase

Temp. calc. (°C)	Temp exp. (°C) [16]	Type	Invariant reaction	x(Ag)	x(Sn)	x(Te)
873.3	…	U1	L1 + γ-Ag$_2$Te → L2 + β-Ag$_2$Te	0.654	0.034	0.312
813.5	…	U2	L + γ-Ag$_2$Te → (Ag) + β-Ag$_2$Te	0.868	0.074	0.058
725.8	716 ± 4	U3	L + (Ag) → β-Ag$_2$Te + ζ-Ag$_4$Sn	0.797	0.168	0.035
583.9	591 ± 3	E1	L1 → L2 + β-Ag$_2$Te + SnTe	0.438	0.229	0.333
533.6	532 ± 3	U4	L + β-Ag$_2$Te → ζ-Ag$_4$Sn + SnTe	0.566	0.387	0.047
486.2	478±2*	P1	L + ζ-Ag$_4$Sn + SnTe → ε-Ag$_3$Sn	0.511	0.468	0.021
434.0	…	P2	L + β-Ag$_2$Te + SnTe → Ag$_x$Sn$_{2-x}$Te$_2$	0.380	0.103	0.517
424.2	-**	U5	L+β-Ag$_2$Te → β-Ag$_{1.9}$Te+Ag$_x$Sn$_{2-x}$Te$_2$	0.380	0.097	0.523
395.5	~380 **	U6	L+β-Ag$_{1.9}$Te → β-Ag$_5$Te$_3$+Ag$_x$Sn$_{2-x}$Te$_2$	0.371	0.084	0.545
386.8	343 ± 10	U7	L + SnTe → (Te) + Ag$_x$Sn$_{2-x}$Te$_2$	0.173	0.108	0.719
330.5	333 ± 1	E2	L → (Te) + β-Ag$_5$Te$_3$ + Ag$_x$Sn$_{2-x}$Te$_2$	0.314	0.059	0.627
221.6	218 ± 2	E3	L → SnTe + ε-Ag$_3$Sn + (Sn)	0.036	0.963	0.001

*The same phases, but univariant reaction was identified in[16]

**These invariant reaction were not established by experiment as the β-Ag$_{1.9}$Te phase was not identified in.[16]
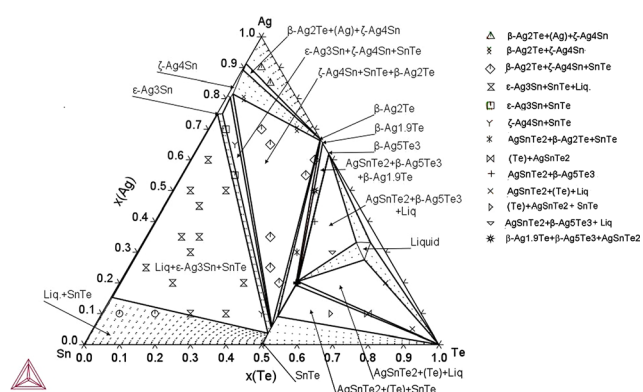
Fig. 18 The isothermal section of the Ag-Sn-Te phase diagram at 350 °C
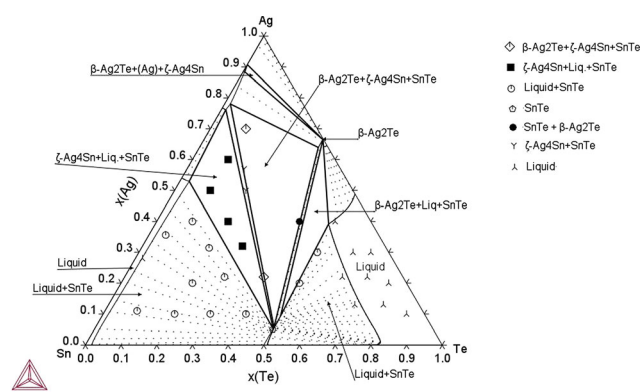

Fig. 19 The isothermal section of the Ag-Sn-Te phase diagram at 500 °C

Chang et al.[18] The calculated liquidus surface is shown in Fig. 28 and compared with results of Chang et al.[18] Small gaps appear in drawn phase diagram near critical points of
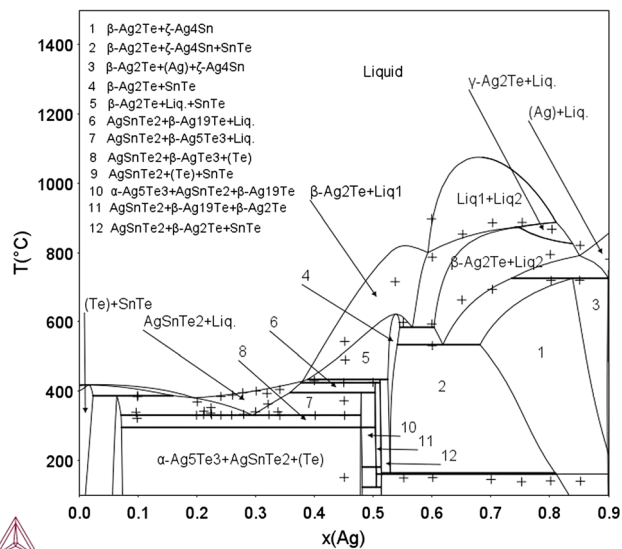

Fig. 20 The isopleth of the Ag-Sn-Te phase diagram for 10 at.% Sn. Experimental data are from Blachnik et al.[16]

the monovariant line and at the isotherms in the case of liqud miscibility gap. Existing software packages cannot completely close the gaps because of small Gibbs energy differences near a critical point. Therefore, the gaps were closed manually, and the approximate position of the critical point is indicated in the Fig. 28.

The calculated invariant reactions containing liquid phase are presented in Table 4. The comparison with experimental values established in the work of Blachnik et al.[16] are included for comparison whenever possible.
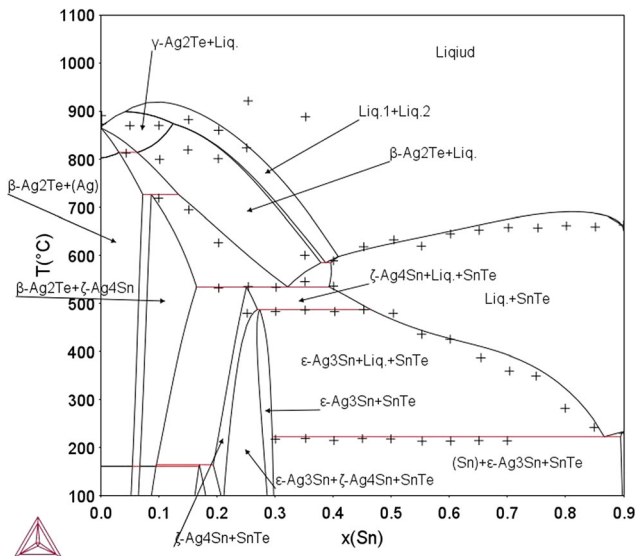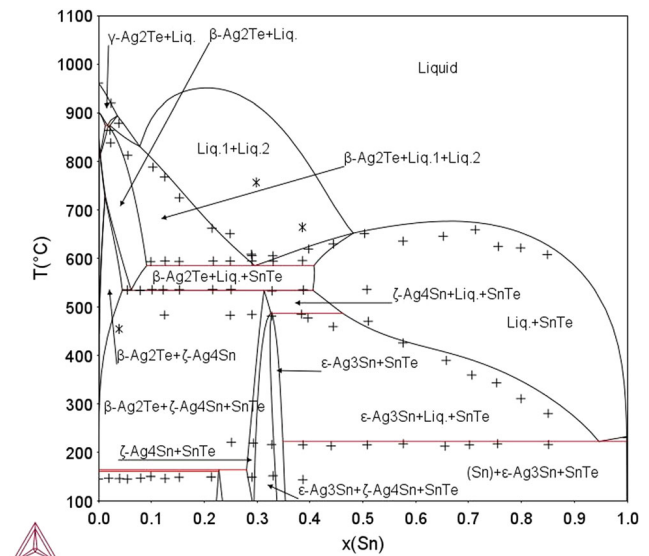
J. Phase Equilib. Diffus. (2022) 43:139–163

159

Fig. 21 The isopleth of the Ag-Sn-Te phase diagram for 10 at.% Te. Experimental data are from Blachnik et al.[16]

Fig. 22 The isopleth of the Ag-Sn-Te phase diagram for 30 at.% Ag. Experimental data are from Blachnik et al.[16]

Fig. 23 The isopleth of the Ag-Sn-Te phase diagram for the Ag₂Te-Sn section. Experimental data are from Blachnik et al.[16]
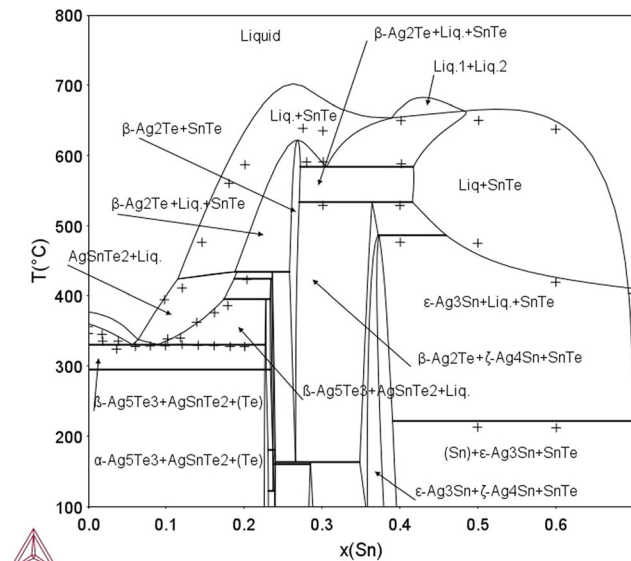

Fig. 24 The concentration dependence of enthalpy of mixing in liquid for the x(Ag)/x(Sn) = 1/4 at a temperature of 887 °C. Experimental data are from Gather et al.[20]. Reference states are pure liquid elements at the temperature of measurements

6 Discussion

The results of the experimental and theoretical part of this study are consistent and very good agreement was reached between the theoretical assessment and other available experimental results.[16-20] The isothermal sections obtained in the experimental program agreed well with the calculations. According to Blachnik and Gather,[16] the eutectic temperature corresponding to the Liq. → (Te) + Ag$_x$Sn$_{2-x}$Te$_2$ + β-Ag$_5$Te$_3$ invariant reaction is 333±1 °C, and the presence of liquid phase was confirmed in the isothermal section at 350 °C. The results of modelling

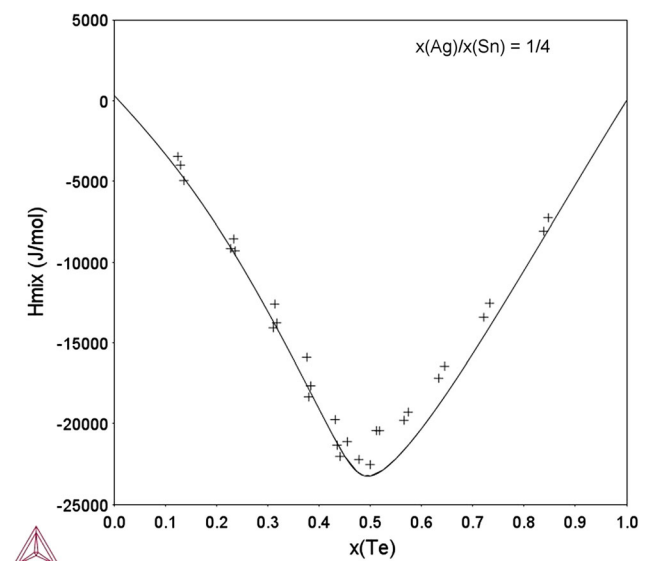confirmed presence of small region of the liquid phase, which does not extend to the binary Ag-Te subsystem. The lowest temperature where liquid is present in binary Ag-Te system is 360.2 °C for x(Te) = 0.663, and no experimental data were obtained to contradict to this theoretical finding in the scope of the experimental part of this study. Also, very good agreement was reached with the experimental isopleth for 10 at.% Sn results from[16] in the Te-rich region (see Fig. 20).
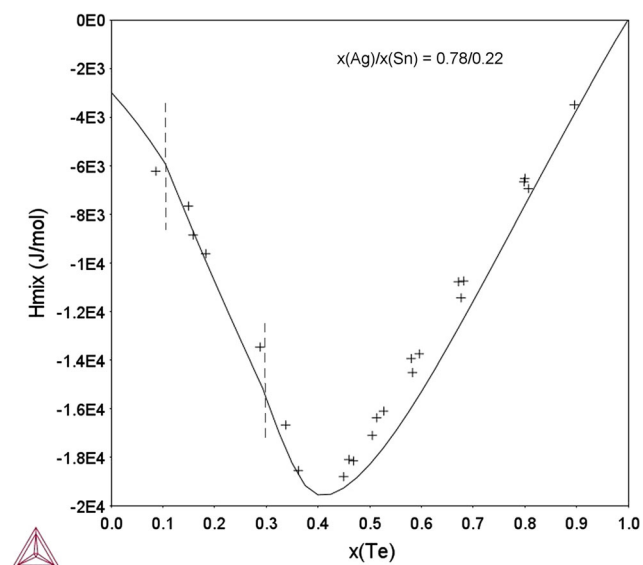
Fig. 25 The concentration dependence of enthalpy of mixing in liquid for the $x(Ag)/x(Sn) = 0.78/0.22$ at a temperature of 887 °C. Experimental data are from Gather et al.[20] The region between dashed lines represents the miscibility. Reference states are pure liquid elements at the temperature of measurements
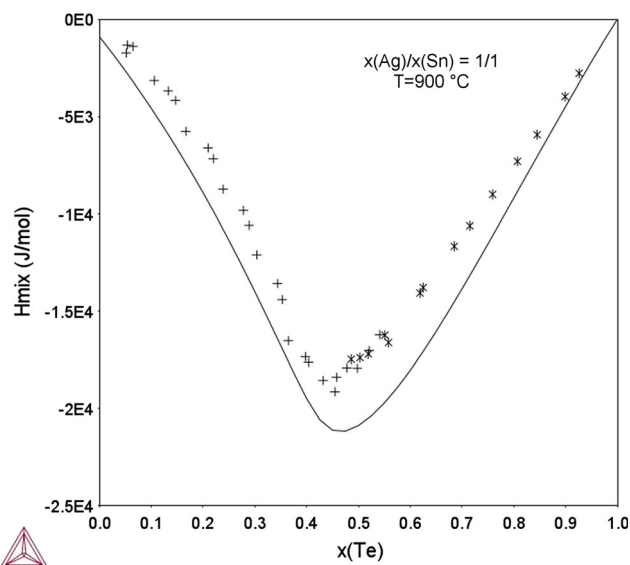

Fig. 27 The concentration dependence of enthalpy of mixing in liquid for the $x(Ag)/x(Sn) = 1/1$ at a temperature of 900 °C. Experimental data are from Römermann et al.[21] Two different runs were carried out during the measurements with different types of element mixing. Reference states are pure liquid elements at the temperature of measurements
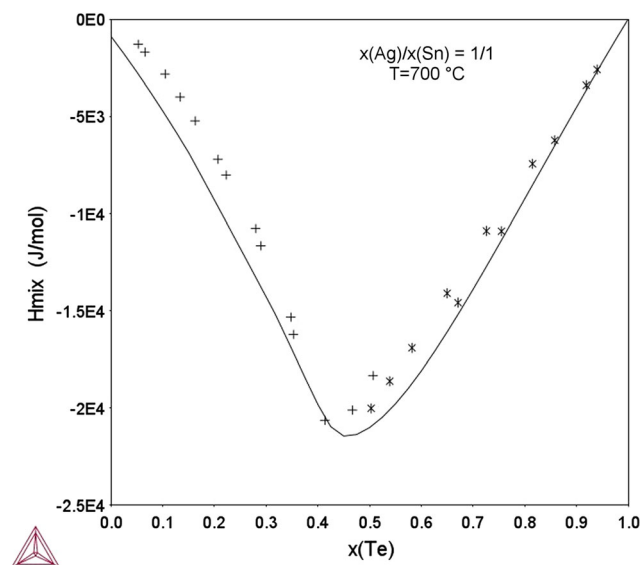

Fig. 26 The concentration dependence of enthalpy of mixing in liquid for the $x(Ag)/x(Sn) = 1/1$ at a temperature of 700 °C. Experimental data are from Römermann et al.[21] Two different runs were carried out during the measurements with different types of element mixing. Reference states are pure liquid elements at the temperature of measurements

Fig. 28 Calculated liquidus surface for the Ag-Sn-Te. Experimental data are from Chang et al.[19]

Our experimental results did not clearly identify the presence of the β-Ag$_{1.9}$Te phase in the ternary samples. This phase was also not found in relevant isopleths in,[16] despite being present in the binary Ag-Te phase diagram in that paper. This can be explained by difficulties connected with identifying and distinguishing this phase from the β-
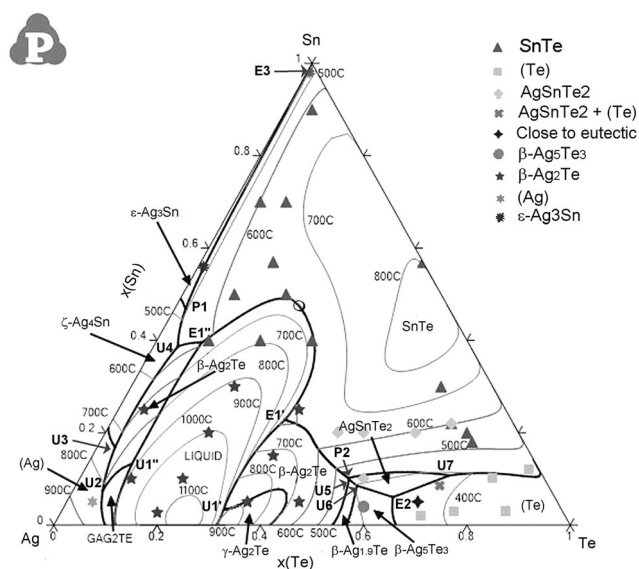
Ag$_2$Te phase. On the other hand, theoretical modelling predicted the projection of β-Ag$_{1.9}$Te phase (see Fig. 18) into the ternary isothermal section at 350 °C despite assuming negligible solubility of Sn in this phase. Preventing the β-Ag$_{1.9}$Te phase to project from the binary Ag-Te edge deeper into the ternary phase diagram requested significantly higher solubilities of Sn in β-Ag$_2$Te and β-Ag$_5$Te$_3$ phases than those found by experiment. Only

in such case small three phase field β-Ag_2Te+ β-$Ag_{1.9}Te$+ β-Ag_5Te_3 would appear adjacent to the Ag-Te binary.

The agreement between the experimental results and calculation at the 500 °C is excellent. There is very good agreement not only for main phase fields but also the experiments and calculation fit very well even for very narrow two-phase fields (e.g. SnTe+ β-Ag_2Te).

New information was obtained in the experimental part of this study. The ternary phase was generally supposed to be stoichiometric with the composition $Ag_{25}Sn_{25}Te_{50}$, but all our experimental measurements of the composition of the ternary phase showed the composition approx. $Ag_{20-}Sn_{30}Te_{50}$ with high degree of reliability. This composition was obtained independently on the type of phase equilibria found in studied samples. Therefore, the model in the thermodynamic assessment was selected with respect to real crystallographic structure of the phase and at the same time, it also allows the mixing of Ag and Sn and the modelling of experimentally measured composition.

The agreement with the experimental isopleths from[16] is also very reasonable. All important features are properly reproduced by the modelling. The principal difference is the presence of phase fields containing $Ag_{1.9}Te$ phase, which is located in Fig. 20 and 22. The disagreement of the calculated size of liquid miscibility gaps in calculated Fig. 21 and 23 and the experimental ones shown in Fig. 4 and 5 in the Ref.[16] exists but the experimentally established boundaries of the miscibility gaps in[16] are uncertain, marked by dashed lines. It is necessary to note here, that some temperatures of invariant reactions in figures in the work[16] are wrong, e.g. the maximal temperatures of the ternary $Ag_xSn_{2-x}Te_2$ phase for 10 at.% Sn and 30 at.% Ag are different and both are wrong and does not correspond to the relevant invariant reaction drawn in isopleths in Fig. 6 and 7 published in.[16]

There is very good agreement between calculated and experimental enthalpies of mixing from.[20] The enthalpy measurements for various Ag/Sn ratios at 887 °C published by Gather and Blachnik[20] are reproduced with excellent agreement especially for Te-poor region. Especially when extrapolating the experimental data towards the values of enthalpies of mixing in the limiting Ag-Sn binary system, the extrapolated ternary experimental values correspond very well to the calculated values in the Ag-Sn system. The theoretical results are slightly more negative for Te-rich region but still the agreement is very good.

As mentioned above worse agreement was obtained for the experimental results of Römermann and Blachnik,[21] especially in the Te-poor region for the temperatures 700, 800 and 900 °C, i.e., the extrapolated values of the experimental data towards the Ag-Sn binary edge do not correspond to the calculated values of enthalpy of mixing in the binary system for all temperatures (see Fig. 26, 27),

but they tend to go rather to the value of 0 J/mol for the composition Ag0.5Sn0.5. According to the Ref[20] the selected standard states should be pure elements in the liquid state at the temperature of measurements. The experimental data published data in Ref[21] were measured in two separate experimental runs (one in the x(Te) > 0.5 region and the second in the x(Te) < 0.5 region). The enthalpy values around x(Te)=0.5, where these two runs overlap, show systematic discrepancies. The results for the x(Te)<0.5 region do not correspond to above mentioned selection of standard states and the standard states of Ag0.5Sn0.5(liq) and Te(liq) are probably valid for the experimental measurements in this region. Unfortunately, the authors definitely used the pure liquid elements standard states during drawing the concentration dependence of the enthalpy of mixing in relevant figure and in further evaluation of the results in work.[21] Therefore, there are significant doubts about validity of this data.

The calculations correctly reproduced the decrease of the exothermic character of the enthalpies of mixing in the Ag-Sn-Te system, but the calculated values are more negative with increasing temperature. Nevertheless, the difference is still reasonably small. In addition, the measured values of enthalpies of mixing seem to be quite similar especially for the temperatures 700 and 800 °C and no clear temperature dependence can be observed in the Te-poor region. Considering also above discussed the uncertainties in the experimental data from,[21] the temperature dependence of the enthalpy of mixing of the liquid was not modelled here.

The calculated liquidus surface of the Ag-Sn-Te system is presented in the Fig. 27. The results are compared with experimental results from Chang et al.[18] and Blachnik and Gather[16]. Both experimentally established liquidus surfaces are very similar and the calculated one correctly reproduced all important features. The important part of the surface is very pronounced region of liquid miscibility gap which reaches beyond 50 at.% of Sn. The ternary phase also existed as primary solidification phase in a certain region in the Te-rich area. Main difference between calculations and experiment was found in this case as the area of primary solidification of the ternary phase is significantly wider in the paper[18] than in[16] and in the theoretical calculations. Here the results from[16] and from the calculation are correct as the area of primary solidification in the paper[18] extends up to the 600 °C, which is not correct both according to the results of our experiments and work.[16] The ternary phase was not found in the isothermal section at 500 °C and it can be estimated that it melted incongruently by the peritectic reaction around 430 °C. As mentioned above, there are some errors in paper,[16] nevertheless this temperature can be reasonably estimated from isopleth presented there. The invariant reactions

162

J. Phase Equilib. Diffus. (2022) 43:139–163

which contain the liquid phase are presented in the Table 4. Here the comparison was made with the results presented in[16] where possible. Not all invariant reactions were found in the experimental work. We mentioned already that β-$Ag_{1.9}Te$ was not identified in the work[16] and therefore some additional reactions were obtained by calculations and some temperatures were influenced by this. Nevertheless, it can be concluded that very good agreement was reached whenever the experimental and calculated invariant reactions could be linked.

7 Conclusion

The Ag-Sn-Te system was studied experimentally and theoretically in the scope of this paper and several new results were obtained. They are generally consistent with results presented in older literature[16–21] and allows for the first time to describe completely this ternary system.

From the experimental point of view, the ternary phase was found to be slightly off presumed composition Ag_{25}-$Sn_{25}Te_{50}$. All our experimental measurements of the composition of the ternary phase showed the composition being close to the. $Ag_{20}Sn_{30}Te_{50}$ with high degree of reliability.

The presence of the liquid phase inside the ternary phase diagram at 350 °C was experimentally confirmed and theoretically modeled in agreement with results from[16].

Complete theoretical assessment was prepared by the *CALPHAD* method, and the theoretical results are in very good agreement with our and literature experimental results.

This work was carried out in the scope of the experimental and theoretical studies of more complex Ag-Pb-Se-Sn-Te system to be able to describe the systems for materials suitable for thermoelectric applications.

References

1. B. Cai, H. Hu, H.-L. Zhuang, and J.-F. Li, Promising Materials for Thermoelectric Applications, *J. Alloys Compd.*, 2019, **806**, p 471-486.

2. A. Allouhi, Advances on Solar Thermal Cogeneration Processes Based on Thermoelectric Devices: a Review", *Sol. Energy Mater. Sol. Cells*, 2019, **200**, p 109954.

3. G. Tan, M. Ohta, and M.G. Kanatzidis, Thermoelectric Power Generation: From New Materials to Devices, *Philos. Trans. R. Soc. A*, 2019, **377**, p 20180450.

4. R. Moshwan, L. Yang, J. Zou, and Z.-G. Chen, Eco-Friendly SnTe Thermoelectric Materials: Progress and Future Challenges, *Adv. Funct. Mater.*, 2017, **27**, p 1703278.

5. Y.Z. Pei, N.A. Heinz, and G.J. Snyder, Alloying to Increase the Band Gap for Improving Thermoelectric Properties of Ag_2Te, *J. Mater. Chem.*, 2011, **21**, p 18256-18260.

6. C.-H. Su, Design, Growth and Characterization of PbTe-Based Thermoelectric Materials, *Prog. Cryst. Growth Charact. Mater.*, 2019, **65**, p 47-94.

7. L. Zhao, J. Wang, J. Li, J. Liu, C. Wang, J. Wang, and X. Wang, High Thermoelectric Performance of Ag Doped SnTe Polycrystalline Bulks via the Synergistic Manipulation of Electrical and Thermal Transport, *Phys. Chem. Chem. Phys.*, 2019, **21**, p 17978-17984.

8. M.H. Lee, D.-G. Byeon, J.-S. Rhyee, and B. Ryu, Defect Chemistry and Enhancement of Thermoelectric Performance in Ag-Doped $Sn_{1+\delta-x}Ag_xTe$, *J. Mater. Chem. A*, 2017, **5**, p 2235-2242.

9. Y. Chen, M.D. Nielsen, Y.-B. Gao, T.- J. Zhu, X. Zhao, and J.P. Heremans, $SnTe–AgSbTe_2$ Thermoelectric Alloys, *Adv. Energy Mater.*, 2012, **2**, p 58-62.

10. J. Wu, J. Yang, H. Zhang, J. Zhang, S. Feng, M. Liu, J. Peng, W. zhu, and T. Zou, Fabrication of Ag-Sn-Sb-Te Based Thermoelectric Materials by MA-PAS and Their Properties, *J. Alloys Compd.*, 2010, **507**, p 167-171.

11. L. Nykyruya, M. Ruvinskiya, E. Ivakinb, O. Kostyuka, I. Horichoka, I. Kisialioub, Y. Yavorskyya, and A. Hrubyaka, Low-Dimensional Systems on the Base of PbSnAgTe (LATT) Compounds for Thermoelectric Application, *Phys. E (Amsterdam Neth)*, 2019, **106**, p 10-18.

12. J. Androulakis, K.-F. Hsu, R. Pcionek, H. Kong, C. Uher, J.J. D'Angelo, A. Downey, T. Hogan, and M.G. Kanatzidis, Nanostructuring and High Thermoelectric Efficiency in p-Type $Ag(Pb_{1-y}Sn_y)_mSbTe_{2+m}$, *Adv. Mater.*, 2006, **18**, p 1170-1173.

13. F.N. Rhines, *Phase Diagrams in Metallurgy: Their Development and Application*. McGraw-Hill, New York, 1956.

14. M. Hillert, *Phase Equilibria, Phase Diagrams and Phase Transformation: Their Thermodynamic Basis*. Cambridge University Press, Cambridge, 1998.

15. V.B. Rajkumar, and S.-W. Chen, Ag-Se Phase Diagram Calculation Associating ab-Initio Molecular Dynamics Simulation, *Calphad*, 2018, **63**, p 51-60.

16. R. Blachnik, G. Bolte, and B. Gather, Ternäre Chalkogenhaltige Systeme V Das Ternäre Phasendiagramm Silber-Zinn-Tellur, *Z. Metallkde.*, 1978, **69**, p 530-533. , **in German**

17. R. Blachnik, and B. Gather, Mischungen Von GeTe, SnTe und PbTe mit Ag2Te. Ein Beitrag zur Klärung der Konstitution der Ternären Ag-IVb-Te systeme (IVb = Ge, Sn, Pb), *J. Less-Common Met.*, 1978, **60**, p 25-32. , **(in German)**

18. J.S. Chang, S.W. Chen, K.C. Chiu, H.J. Wu, and J.J. Chen, Liquidus Projection of the Ag-Sn-Te Ternary System, *Metall. Mater. Trans. A*, 2014, **45A**, p 3728-3740.

19. B. Gather, and R. Blachnik, Ag8SnTe6 Ein Neuer Stabiler Vertreter der Argyrodite?, *Z. Naturforsch. A Phys. Sci.*, 1983, **38**, p 786-787. , **(in German)**

20. B. Gather, and R. Blachnik, Mischungsenthalpien in Ternären Systemen V: Das System Silber-Zinn-Tellur, *Z. Met.*, 1986, **77**, p 643-648. , **(in German)**

21. F. Römermann, and R. Blachnik, The Excess Enthalpies of Liquid Ag-Ge-Te and Ag-Sn-Te Alloys, *Z. Met.*, 2001, **92**, p 336-344.

22. Y. Liu, D. Liang, and L. Zhang, Thermodynamic Descriptions for the Sn-Te and Pb-Sn-Te Systems, *J. Electron. Mater.*, 2010, **39**, p 246-257.

J. Phase Equilib. Diffus. (2022) 43:139–163

163

23. C.-S. Oh, J.-H. Shim, J.-H. Lee, and B.-Y. Lee, A Thermodynamic Study on the Ag-Sb-Sn System, *J. Alloys Compd.*, 1996, **238**, p 155-166.

24. W. Gierlotka, The Thermodynamic Assessment of the Ag-Te System, Private Communication.

25. N. Saunders, and A.P.P. Miodownik, *CALPHAD (Calculation of Phase Diagrams): A Comprehensive Guide*. Elsevier Ltd, New York, 1998.

26. H. Lukas, S.G. Fries, and B. Sundman, *Computational Thermodynamics: The Calphad Method*. Cambridge University Press, New York, 2007.

27. J.-O. Andersson, T. Helander, L. Höglund, P. Shi, and B. Sundman, Thermo-Calc & DICTRA, Computational Tools for materials Science, *Calphad*, 2002, **26**, p 273-312.

28. W. Cao, S.-L. Chen, F. Zhang, K. Wu, Y. Yang, Y.-A. Chang, R. Schmid-Fetzer, and W.A. Oates, PANDAT Software with PanEngine, PanOptimizer and PanPrecipitation for Multicomponent Phase Diagram Calculation and Materials Property Simulation, *Calphad*, 2009, **33**, p 328-342.

29. A. Dinsdale, SGTE Data for Pure Elements, *Calphad*, 1991, **15**, p 317-425.

30. SGTE Unary Database, ver. 5.0. www.sgte.net/en/free-pure-substance-database.

31. O. Redlich, and A.T. Kister, Thermodynamics of Nonelectrolyte Solutions—x-y-t Relations in a Binary System, *Ind. Eng. Chem.*, 1948, **40**, p 341-345.

32. Y.M. Muggianu, M. Gambino, and J.P. Bros, Enthalpies of Formation of Liquid Alloys Bismuth-Gallium-Tin at 723 K–choice of Analytical Representation of Integral and Partial Thermodynamic Functions of Mixing for this Ternary System, *J. Chim. Phys.*, 1975, **72**, p 83-88.

33. A. Dinsdale, A. Kroupa, A. Watson, J. Vrestal, A. Zemanova, and P. Broz, MP0602 HT SOLDERS database, COST MP0602 Action (2012)

34. R.M. Honea, Empressite and Stuetzite Redefined, *Am. Miner.*, 1964, **49**, p 325-338.

35. A. Watson, Private Report, COST 531 Action, (2008)

36. H. Flandorfer, C. Luef, and U. Saeed, On the Temperature Dependence of the Enthalpies of Mixing in Liquid Binary (Ag, Cu, Ni)-Sn Alloys, *J. Non. Cryst. Solids.*, 2008, **354**, p 2953-2972.

37. P.Y. Chevalier, Unpublished Work, (2005)

38. W. Gierlotka, "Thermodynamic Assessment of the Ag–Te Binary System, *J. Alloys Compd.*, 2009, **485**, p 231-235.